Acta Oceanol. Sin., 2024, Vol. 43, No. 3, P. 66–86
https://doi.org/10.1007/s13131-023-2284-5
http://www.aosocean.com
E-mail: ocean2@hyxb.org.cn

The environmental analysis and site selection of mussel and large yellow croaker aquaculture areas based on high resolution remote sensing

Lina Cai[1], Jie Yin[1], Xiaojun Yan[1]*, Yongdong Zhou[2], Rong Tang[1], Menghan Yu[1]

[1] Marine Science and Technology College, Zhejiang Ocean University, Zhoushan 316022, China

[2] Zhejiang Marine Fisheries Research Institute, Zhejiang Ocean University, Zhoushan 316004, China

Received 6 June 2023; accepted 8 December 2023

Abstract

Mussel aquaculture and large yellow croaker aquaculture areas and their environmental characteristics in Zhoushan were analyzed using satellite data and *in-situ* surveys. A new two-step remote sensing method was proposed and applied to determine the basic environmental characteristics of the best mussel and large yellow croaker aquaculture areas. This methodology includes the first step of extraction of the location distribution and the second step of the extraction of internal environmental factors. The fishery ranching index (FRI1, FRI2) was established to extract the mussel and the large yellow croaker aquaculture area in Zhoushan, using Gaofen-1 (GF-1) and Gaofen-6 (GF-6) satellite data with a special resolution of 2 m. In the second step, the environmental factors such as sea surface temperature (SST), chlorophyll *a* (Chl-*a*) concentration, current and tide, suspended sediment concentration (SSC) in mussel aquaculture area and large yellow croaker aquaculture area were extracted and analyzed in detail. The results show the following three points. (1) For the extraction of the mussel aquaculture area, FRI1 and FRI2 are complementary, and the combination of FRI1 and FRI2 is suitable to extract the mussel aquaculture area. As for the large yellow croaker aquaculture area extraction, FRI2 is suitable. (2) Mussel aquaculture and the large yellow croaker aquaculture area in Zhoushan are mainly located on the side near the islands that are away from the eastern open waters. The water environment factor template suitable for mussel and large yellow croaker aquaculture was determined. (3) This two-step remote sensing method can be used for the preliminary screening of potential site selection for the mussels and large yellow croaker aquaculture area in the future. the fishery ranching index (FRI1, FRI2) in this paper can be applied to extract the mussel and large yellow croaker aquaculture areas in coastal waters around the world.

Key words: mussel aquaculture area, large yellow croaker aquaculture area, high resolution satellite, site selection, environmental analysis

Citation: Cai Lina, Yin Jie, Yan Xiaojun, Zhou Yongdong, Tang Rong, Yu Menghan. 2024. The environmental analysis and site selection of mussel and large yellow croaker aquaculture areas based on high resolution remote sensing. Acta Oceanologica Sinica, 43(3): 66–86, doi: 10.1007/s13131-023-2284-5

1 Introduction

Marine ranching was developed based on the "cultivated fishery" concept developed in the 1960s in Japan (Yang et al., 2016; Ma and Yang, 1994; Chang, 1985). In 1965, Chengkui Zeng, an academician of the Chinese Academy of Sciences, put forward the idea of developing ocean "aquaculture" for planting algae and shellfish, and "ranching" for fish and shrimp, to achieve the goal of "cultivating the sea" (Sun, 2005). The concept of building Chinese marine ranching was put forward in 1981, as marine ranching is capable of restoring fishery resources and expanding the space for fishery activities (Yu and Wang, 2015). The National Development and Reform Commission, the Ministry of Agriculture of the People's Republic of China, and the State Oceanic Administration have allocated funds to carry out marine ranching demonstration areas in coastal areas of China every year to vigorously promote the construction of Chinese marine ranching in recent years (Reporter, 2020).

Some China national marine ranching demonstration zones have been established in Zhoushan by the end of 2022. Among them, notable examples include the Zhoushan Shengsi mussel aquaculture area and the Zhoushan Putuo Dongji large yellow croaker cage aquaculture area. This paper focuses on the aforementioned two marine aquaculture zones as specific research areas, aiming to investigate the utilization of satellite technology for observing marine ranching activities in Zhoushan.

Satellite remote sensing plays an important role in aquaculture area management. Many methods utilizing satellite technology have been developed to extract information from aquaculture areas (Zhang et al., 2013, 2020; Sui et al., 2020; Ottinger et al., 2017; Massarelli et al., 2021). The object-based region growing edge detection (OBRGIE) method and the object merging index (OMI) method were proposed as approaches to extract coastlines near marine aquaculture areas. OBRGIE is used for coastline extraction and OMI is used for providing edge information

Foundation item: The National Key Research and Development Program of China under contract Nos 2023YFD2401900 and 2020YFD09008004; the National Natural Science Foundation of China Key International (Regional) Cooperative Research Project under contract No. 42020104009; the Basic Public Welfare Research Program of Zhejiang Province under contract No. LGF21D010004.
*Corresponding author, E-mail: yanxj@zjou.edu.cn

and segmentation results (Zhang et al., 2013). In terms of aquaculture area extraction, Sui et al. proposed an automatic aquaculture area extraction method based on semantic segmentation to solve the problem of low recognition rate of traditional feature extraction methods in some cases (Sui et al., 2020; Zhang et al., 2013). In addition, Zhang et al. (2020) extracted Marine raft aquaculture areas in Sentinel-1 images by a segmentation network combined with non-subsampled contourlet transform (NSCT) . Furthermore, digital elevation model (DEM) data and accurate coastline data were analyzed to obtain topographic information to identify and conceal potential marine aquaculture areas with high accuracy (83%) (Ottinger et al., 2017). Meanwhile, high-resolution images were used to extract mussel aquaculture areas by combining adaptation-sharpen filters and color correction (Massarelli et al., 2021).

Previous studies on aquaculture have focused on the exploration of environmental factors or only on how to extract aquaculture areas and coastlines. In addition, the site selection of aquaculture areas only focuses on selecting suitable aquaculture areas by comparing the environmental differences between aquaculture areas and non-aquaculture areas, and there are not many environmental factors considered, which leads to the deviation between the site selection opinions and the actual situation. There are few studies on extracting existing aquaculture areas as environmental templates before site selection. Many Chinese high-resolution satellites were launched successfully in recent years and have made great progress in ocean applications (Yuan et al., 2018). Gaofeng-6 (GF-6) satellite has a resolution of 2 m in the panchromatic band and 8 m in the multispectral band and can observe the floating infrastructure of aquaculture facilities and extract the environmental characteristics of surrounding waters. Therefore, it is necessary to develop the techniques and methods of aquaculture extraction. For aquaculture to be successful, it is necessary to monitor the marine water environmental factors (Perkins, 2019; Li et al., 2021b). Remote sensing technology in water environment monitoring is mainly based on the color difference and water spectral reflectance difference to detect eutrophication (Li et al., 2006) and other characteristics of water quality. Many satellite data including Sentinel-3 Sentinel-3 Ocean and Land Colour Instrument (OLCI) (Blix et al., 2018), Moderate-resolution Imaging Spectrorad iometer (MODIS) (Yu et al., 2016), Landsat Thematic mapper (TM) and operational land imager (OLI) (Ye and Song, 2020), Chinese high-resolution satellite series (Zhai et al., 2021), and many other satellite data (De Mendonça et al., 2017) were applied to retrieve water environmental parameters based on algorithms (Yang et al., 2017) using visible and near-infrared bands.

As the largest fishing ground in China, Zhoushan developed many mussel aquaculture areas and large yellow croaker aquaculture areas. This study focuses on mussel aquaculture and the large yellow croaker aquaculture area in the Shengsi Gouqi Island area and Zhongjieshan Islands area of Dongji Town. These areas were previously identified by the Ministry of Agriculture and Rural Affairs, PRC as the demonstration marine ranching areas, mainly for mussels (*Mytilus couscous*) and large yellow croakers (*Larimichthys crocea*). Gouqi Island is famous for mussel (*Mytilus couscous*) aquaculture. Zhongjieshan Islands are important places for the growth, fishing, and reproduction of the main economic fish such as the large yellow croaker. They are of important economic value in the Zhoushan sea area of Zhejiang Province.

The main mussel varieties in Zhoushan aquaculture are *M. couscous* and *M. edulis* (Wong and Levinton, 2004). *Mytilus couscous* belongs to Mollusca, Bivalvia, Mytiloida, Mytilidae, and *Mytilus*, commonly known as mussels, and is a warm water species (Li et al., 2021a; Zhang, 2009), is one of the unique mussel species in the Zhoushan sea area (Wong and Levinton, 2004; Yang and Zhou, 1998). *Larimichthys crocea* belongs to Perciformes, Sciaenidae, *Larimichthys* genus. It is one of the four traditional Chinese seafood delicacies (Chen, 2011).

In this paper, aquaculture mainly includes mussel and large yellow croaker aquaculture areas. This research aims to develop a method based on remote sensing for the detection and management of mariculture areas in Zhoushan and other similar areas. We developed a new fishery ranching index (FRI) for Zhoushan mussel and large croaker aquaculture area extraction, which is shown in Section 2. Zhoushan aquaculture environmental factors such as chlorophyll *a* (Chl-*a*) concentration, suspended sediment concentration (SSC), and sea surface temperature (SST) are also analyzed in Section 3. Section 4 discusses the potential aquaculture area site selection for the future. The conclusions are performed in Section 5.

2 Materials and methods

2.1 *Study area*

Zhoushan, the largest archipelago in China, is located between 29°32′–31°04′N and 121°30′–123°25′E (Song, 2001) in the northeast of Zhejiang Province, south of the Changjiang River (Yangtze River) Estuary, and on the outer edge of Hangzhou Bay on the East China Sea (Fig. 1). Zhoushan fishery, located in the south of the Changjing River Estuary along the western Pacific coast, is an important part of the fishery in the East China Sea, where the water quality is fertile, the bait species are rich, the hydrologic environment is suitable, and it is a good area for the reproduction, baiting and growth of various aquatic organisms (Yu et al., 2010). There are many islands and reefs in the sea area, and the hydrologic environment of the Zhoushan sea area is complex (Hu, 2020). Runoff, tides, waves, and coastal currents are strongly affected by the Taiwan Warm Current, Kuroshio branching, and upwelling (Hu, 2007). The estuaries of nearby rivers bring abundant nutrients and bait to Zhoushan. The bottom of the sea is mainly composed of silty and clayey ooze, suitable for fish habitat and reproduction. In addition, nutrients in the Zhoushan sea area also come from the resuspension of sediments induced by the interaction of tidal currents and the ocean floor (Song, 2001). The upwelling, induced by topography and monsoon, also brings nutrients to the sea surface (Song, 2001). Under the comprehensive influence of various factors, Zhoushan has become a famous “fishing barn in the East China Sea”. In recent years, with the popularization of the concept of aquaculture and the strong support of government policies, Zhoushan’s aquaculture has developed rapidly.

Zhoushan Ma’an Archipelago sea area and Zhongjieshan Archipelago sea area are both the first batch to be selected for the National Aquaculture Demonstration Area (Fig. 1). Zhoushan has a long history of mussel aquaculture and vast mussel aquaculture areas, among which Shengsi is the most famous for mussels (Fig. 1). Since 1973, Shengsi mussels have been cultured artificially and mussel aquaculture gradually developed into a pillar industry. As the main producing area of Shengsi mussels, Gouqi Island was named “Mussel Town of Zhejiang Province” by Zhejiang Provincial Marine Fishery Bureau as early as 2001, and “Mussel Town of China” by Zhoushan Chinese Fishery Association in 2010 (Zhang, 2009; Wong and Levinton, 2004; Yang and Zhou, 1998). Taking the yield of mussels in Shengsi in 2015 as an

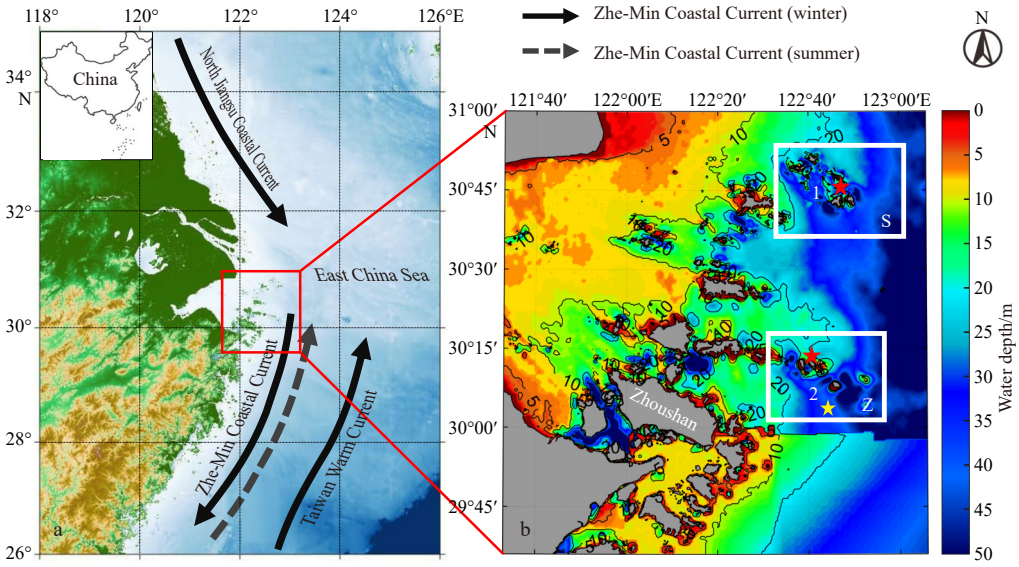

Fig. 1. The location of Zhoushan Islands. Point 1: Zhoushan Gouqi Island. S: Zhoushan Ma'an Archipelago sea area. Point 2: Zhoushan Qingbang Island. Z: Zhongjieshan Archipelago sea area of Dongji Town. The red marks are the locations of the two national aquaculture demonstration zones in Zhoushan. The yellow mark is the sampling point of *in-situ* current data. The map on the top left downloaded from http://211.159.153.75/, with figure number of GS(2023)2764.

example, the yield of mussels in Gouqi Township accounted for about 59% of the total output in Zhoushan Shengsi (Yang and Zhou, 1998). Chinese Gouqi Island is the largest island in the Shengsi Ma'an island chain of Zhoushan. It is a traditional mussel aquaculture area (Fig. 1). The Zhongjieshan Archipelago is an important place for the growth, feeding, and reproduction of the main economic fish in China, as well as the main fishing area. Around Qingbang Island, there are cages for large yellow croaker aquaculture (Fig. 1).

2.2 *Satellite data*

2.2.1 *GF-1 and GF-6 satellite data*

In this study, high-resolution satellite data from China was applied to extract the mussel aquaculture areas and large yellow croaker cage aquaculture areas in Zhoushan. GF-1 and GF-6 satellites were selected in this study due to their 2 m panchromatic and 8 m resolution multi-spectral (PMS) camera and four bands 16 m resolution multi-spectral wide field-of-view (WFV) camera sensors. The fused image can achieve a remarkable 2 m resolution, enabling a more effective extraction of the aquaculture zones.

As the first high-resolution earth observation satellite of China, GF-1 has greatly improved the self-sufficiency rate of high-resolution data in China and improved the timeliness of monitoring. It was successfully launched on April 26, 2013, carrying a 2 m panchromatic and 8 m resolution multi-spectral camera and four bands 16 m resolution multi-spectral wide field-of-view camera (Table 1) (Jia et al., 2016). GF-1 plays an important role in surveying and mapping, marine geographic and climate, weather, water conservancy, forestry resources monitoring, city, and traffic fine management, epidemic situation assessment, and public health emergency as well as earth science research (Bai, 2013).

GF-6 satellite was launched on June 2, 2018, at China Jiu Quan Satellite Launch Center (Wang, 2018). It is a high-resolution satellite for precision agriculture observation in China (Zhang and Chen, 2021) with a 2 m panchromatic and 8 m multi-spectral high-resolution camera (PMS), a multi-spectral medium-resolution wide-range camera (Table 2) (Han et al., 2021a).

Table 1. GF-1 satellite payload parameters

Sensor	Band No.	Spectral range/μm	Spatial resolution/m
PMS	1	0.45–0.90	2
PMS	2	0.45–0.52	8
PMS	3	0.52–0.59	8
PMS	4	0.63–0.69	8
PMS	5	0.77–0.89	8
WFV	1	0.45–0.52	16
WFV	2	0.52–0.59	16
WFV	3	0.63–0.69	16
WFV	4	0.77–0.89	16

A total of 15 GF-1 WFV images were obtained from the archive of the China Resources Satellite Data and Application Center (CRESDA) covering a period during 2017 to 2020.

2.2.2 *HY-1C satellite data*

The Chinese HY-1C watercolor remote sensing satellite has gained prominence since its deployment due to its high spatial resolution, global coverage capability, extended observation duration, and data diversity. Chlorophyll *a* (Chl-*a*) distribution patterns in the Zhoushan mussel aquaculture area and large yellow croaker cage aquaculture area can be retrieved from HY-1C coastal zone image (CZI) to provide a comprehensive analysis of the aquatic environmental characteristics within the Zhoushan marine aquaculture region.

HY-1C, equipped with a Chinese Ocean Color and Temperat-

Table 2. GF-6 satellite payload parameter

Sensor	Band No.	Spectral range/μm	Spatial resolution/m	Width/km
PMS	1 (Pan)	0.45–0.90	2	>90
PMS	2 (blue)	0.45–0.52	8	>90
PMS	3 (green)	0.52–0.59	8	>90
PMS	4 (red)	0.63–0.69	8	>90
PMS	5 (NIR)	0.77–0.89	8	>90

Note: Pan, panchromatic; NIR, near infrared.

ure Scanner (COCTS), a CZI, an automatic identification system for ships, an onboard calibration spectrometer, and an ultraviolet imager (Guo, 2018) (Table 3), was successfully launched on September 7, 2018. It is the third Chinese ocean-color satellite and the first Chinese civil ocean service satellite (Liang,2018). The sensors on the satellite can be used to quantitatively detect chlorophyll and other ocean-color factors. The data of HY-1C CZI can be divided into four levels. L1A: 1–4 band Digital Number (DN) values; L1B: 1–4 band zenith radiance; L2A: Basic product; L2B: standard products (ocean-color elements, SST); L2C: experimental products (ocean-color elements); L3A: ocean-color, water temperature, single day mesh products (SST); L3B: multi-day statistical average; L4A: single-day multi-source fusion products; L4B: fusion products on average for many days. Among which, HY-1C CZI L1B data was applied to obtain Chl-*a* concentration in this paper, and a total of 12 HY-1C CZI images from the website of the National Satellite Ocean Application Service (NSOAS) covering a period during 2019 to 2021 were analyzed.

2.2.3 *Landsat-8 satellite data*

Landsat-8 is the eighth Landsat satellite launched by the United States in 2013 (Loveland and Irons, 2016) carrying an OLI and thermal infrared sensor (TIRS) (Barsi et al., 2014) (Table 4). The temperature of the study area was retrieved from a thermal infrared band of Landsat-8 (Roy et al., 2014).

The utilization of Landsat 8 satellite for sea surface temperature retrieval is motivated by its high spatial resolution, multiband capability, regular observation schedule, long-term data archive, and open data access. These features make it an ideal tool for monitoring sea surface temperatures in the study area, offering a convenient, accurate, and effective data source for scientific research.

Landsat 8 images from the United States Geological Survey (USGS) were archived with the date covering a period during 2017 to 2019.

2.3 *In situ data*

2.3.1 *Investigation of aquaculture*

Mussel aquaculture areas consist of a series of white buoys arranged in neat rows. A rope is attached to the bottom of each buoy. These buoys line up neatly around the island (Fig. 2b). Young mussels were attached to the rope and were harvested during the ripe season. The Dongji Town has a few large yellow croaker aquaculture areas, where located around the Qingbang Islands (Fig. 2c).

The mussel aquaculture area is mainly made of foam plastic, while the large yellow croaker aquaculture area is mainly made of the cage, which is also made of plastic. The extraction of Zhoushan aquaculture information is to extract the information of these arranged floats. The mussel aquaculture area is composed of a large number of neatly arranged lines. There are 10 rows in each line, each row length is 102 m, and the interval width is 4 m (Fig. 2b). Floats are arranged in a row, and a rope about 3 m long is tied under each float. Thick-shell mussels are mainly cultivated in the Gouqi Island area. Seedlings are cultivated in the spring and harvested in autumn two years later.

There are 52 survey points on Zhoushan aquaculture, including 40 for the mussel aquaculture area and 12 for the large yellow croaker aquaculture area, obtained from July 25, 2020 to August 13, 2021, in the study area have been investigated and used for validation of aquaculture detection algorithm.

2.3.2 *Current data of aquaculture*

The tidal current of the study area (south part in Zhoushan fishery) (Fig. 1) from 00:00 on August 29, 2020 to 24:00 on August 31, 2020, was detected using a direct reading ammeter Kuolong-Acoustic Doppler Current Profiler (ADCP) to qualitatively analyze the changing regularity of tidal current and direction.

ADCP is a kind of current meter, using the acoustic Doppler velocity measurement principle and vector synthesis method. ADCP is an instrument for measuring the vertical profile distribution of flow velocity. The velocity and flow direction of several layers on a profile can be measured at one time (Han et al., 2021b). During field measurement, ADCP emits short pulses of fixed-frequency sound waves into the water, scattering them after encountering obstacles, and calculating the velocity and flow direction based on the frequency change of the sound waves when they return (Cui and Zhao, 2005).

2.4 *Other data*

In this paper, the information about typhoon data is from the National Meteorological Science Data Center (http://data.cma.cn/), China Weather Net (http://www.weather.com.cn/), and Zhejiang Province meteorological observatory; the information about the data of red tides is from China ocean information network (https://www.nmdis.org.cn/).

2.5 *Data processing*

2.5.1 *GF-1 and GF-6 data*

The preprocessing of GF Series of satellites PMS data includes radiometric calibration (Yan and Chen, 2021), Fast Line-of-sight Atmospheric Analysis of Spectral Hypercubes (FLAASH) atmospheric correction (Cheng et al., 2011), orthophoto correction, and Nearest Neighbor Diffusion Pan Sharpening (Ma et al., 2018; Yang, 2020). Radiometric calibration of remote sensing is the processing process of converting the gray value (DN value) of remote sensing data recorded by the sensor into radiance value, which is the most basic radiometric correction processing. The role of radiometric calibration is to ensure the accuracy of the detector can meet the application requirements ensure that the output of the detector can reflect the real change of the measured target, and correct the influence of the natural decay of the detector performance on the measured results. Radiometric calibration is necessary for quantitative remote sensing (Wang et al., 2020). Compared with the land, the reflectivity of the water body

Table 3. HY-1C Satellite payload parameters

Sensor	Band No.	Spectral range/μm	Spatial resolution/m
CZI	1	0.42–0.50	50
CZI	2	0.52–0.60	50
CZI	3	0.61–0.69	50
CZI	4	0.76–0.89	50

Table 4. Landsat-8 Satellite payload parameters

Sensor	Band No.	Spectral range/μm	Spatial resolution/m
OIL	1	0.49–0.45	30
OIL	2	0.45–0.51	30
OIL	3	0.53–0.59	30
OIL	4	0.64–0.67	30
OIL	5	0.85–0.88	30
OIL	6	1.57–1.65	30
OIL	7	2.11–2.29	30
OIL	8	0.50–0.68	15
OIL	9	1.36–1.38	30
TIRS	10	10.60–11.19	100
TIRS	11	11.50–12.51	100

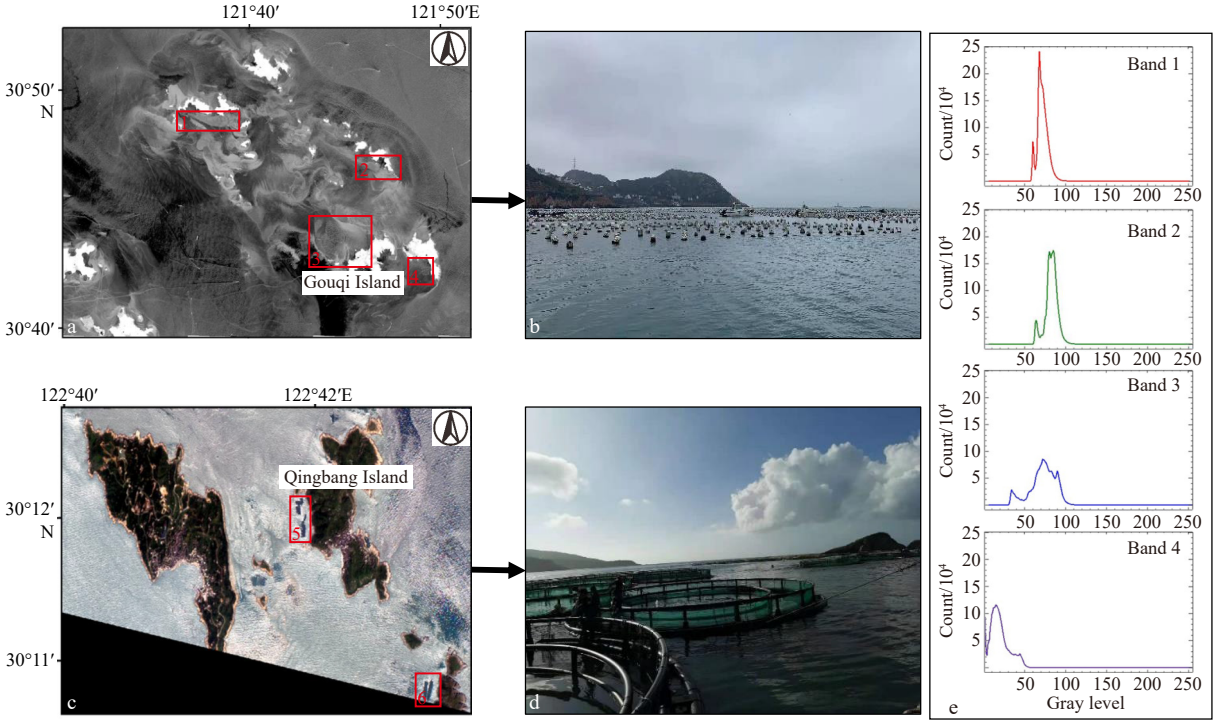

Fig. 2. Location of Zhoushan aquaculture area (a and c), a photograph of the mussel aquaculture area in Shengsi, Zhoushan (b), a photograph of large yellow croaker cages near Qingbang Island in Zhoushan (d), and histogram of GF-6 images (March 3, 2019) in 4 bands (e). Four red squares (1, 2, 3, 4) in a: Zhoushan mussel aquaculture area in Shengsi. Two red squares (5, 6) in c: Qingbang Island large yellow croaker aquaculture area in Zhoushan.

is very low, and the interference information from the atmosphere is in the radiance. Therefore, in remote sensing research of the water environment, accurate atmospheric correction is very important for quantitative inversion of water quality parameters (Yang et al., 2006).

Panchromatic data and multispectral data images are different. Remote sensing image fusion can centralize useful information from multiple sources and fuse them into a single image. It is convenient for a variety of information to complement each other, reducing the ambiguity and uncertainty of the recognition image, and laying the foundation for fast and accurate recognition and extraction of ground object information (Li et al., 2019). Therefore, in the process of preprocessing, orthorectification is carried out for panchromatic data and multispectral data images respectively, and then image registration and image fusion are carried out (Wang et al., 2020; Sun et al., 2016; Zang, 2018). FLAASH atmospheric correction was performed to eliminate the influence of the atmosphere. Remote sensing image is affected by sensor observation angle and ground elevation, which will cause image deformation, it is necessary to ortho-correct the image (Dinguirard and Slater, 1999).

Based on the preprocess above, SSC was retrieved from GF-1/6 PMS images using the model (Eq. (1)) provided in a prior study (Yao et al., 2020). SSC is one of the most important water quality parameters and plays an important role in the study of water and sediment transport in coastal waters and coastal engineering construction.

$$\mathrm{SSC} = 1\,420\left(\frac{\mathrm{B4}}{\mathrm{B1}}\right)^3 - 1\,902.3\left(\frac{\mathrm{B4}}{\mathrm{B1}}\right)^2 + 2\,337.5\,\frac{\mathrm{B4}}{\mathrm{B1}} - 268.43, \quad (1)$$

where SSC is the suspended sediment concentration (mg/L), and B1 and B4 are the remote sensing reflectance of the first (blue) and the fourth (near infrared, NIR) bands of GF-1/6 Satellite after preprocessing, respectively.

2.5.2 *Landsat-8 data*

SST of the mussel and large yellow croaker aquaculture areas can be obtained from the thermal infrared band of Landsat-8 satellite images. the radiative transfer model (RTM) (Xu, 2015) was selected with higher accuracy for the SST inversion of Zhou shan aquaculture.

Firstly, radiometric calibration can turn a DN image into a radiance image. The following is the calculation Eq. (2) for the radiometric calibration.

$$L\left(T_{\mathrm{sensor}}\right) = \mathrm{DN} \cdot G_{\mathrm{ain}} + h, \quad (2)$$

where DN is the gray value, h is the offset, and G_{ain} is the absolute scaling coefficient gain. The above data can be obtained from the thermal infrared data header file of Landsat-8 (Qin et al., 2001; Wang et al., 2015).

Then, the blackbody radiation and brightness temperature inversion were performed. According to the thermal infrared radiation transfer model, the brightness of surface radiation $L(T_{\mathrm{s}})$ can be expressed as the following formula (Chen et al., 2018a).

$$L(T_{\mathrm{s}}) = \frac{L(T_{\mathrm{sensor}}) - L_{\mathrm{up}}}{\tau\varepsilon} - \frac{1-\varepsilon}{\varepsilon}L_{\mathrm{down}}, \quad (3)$$

$$\mathrm{SST} = \frac{\mathrm{K2}}{\ln[1 + \mathrm{K1}/L(T_{\mathrm{s}})]}, \quad (4)$$

where L_{up} is the effective bandpass upwelling radiance and L_{down}

is the effective bandpass downwelling radiance; ε is the sea surface emissivity; τ is the atmospheric path transmittance from the sensor to the target; T_{sensor} is the band average atmospheric transmission; Kl and K2 are model coefficients; ln stands for the natural logarithm, where the base "e" is utilized, representing the mathematical constant known as Euler's number. This set of data was obtained by Atmospheric Correction Parameter Calculator (https://atmcorr.gsfc.nasa.gov/).

Model coefficients K1 and K2 can be obtained from the Landsat-8 data header file. For the tenth band, K1 is 774.885 3 and K2 is 1 321.078 9 respectively.

Chl-*a* concentration of Zhoushan aquaculture can be obtained from the OIL of Landsat-8 satellite images. The Chl-*a* concentration inversion model is shown below (Cai et al., 2022; Huang et al., 2016).

$$\text{Chl-}a = 124.3 \times (\text{B4})^2 + 15.28 \times (\text{B4}) + 0.914, \tag{5}$$

where B4 is the remote sensing reflectance of the fourth bands of Landsat-8 after preprocessing.

2.5.3 *HY-1C data*

For a more comprehensive analysis of regional environmental characteristics, HY-1C satellite CZI data was also applied in this paper. Chl-*a* concentration data, with different spatial resolution and different times compared with Landsat-8 satellite images, were obtained using the HY-1C satellite CZI sensor standard product (Level 1B product). The research data on chlorophyll concentration in this paper are from the secondary products of the China Ocean Satellite Data Service Platform (https://osdds.nsoas.org.cn/#/). The following is the inversion formula of the HY-1C satellite chlorophyll concentration standard data product (Teng et al., 2022).

$$C = 10^{a_0 + a_1 X_1^2 + a_2 X_2^{0.5}}, \tag{6}$$

$$X_1 = \frac{R_{\text{rs}}(\lambda_3)}{R_{\text{rs}}(\lambda_2)}, \tag{7}$$

$$X_2 = \frac{R_{\text{rs}}(\lambda_2)}{R_{\text{rs}}(\lambda_1)}, \tag{8}$$

where C is the concentration of Chl-*a*; a_0, a_1, and a_2 are the parameters of the mode, a_0 = –1.653, a_1 = 0.131, and a_2 = 1.668; λ_1, λ_2, and λ_3 are the wavelengths of the first, second and third bands of CZI, respectively; R_{rs} is remote sensing reflectance (Teng et al., 2022).

2.6 *Methods of extracting Zhoushan aquaculture*

2.6.1 *Zhoushan aquaculture sensitive band*

In the satellite image, Zhoushan aquaculture characteristics as well as histograms in GF-6 PMS fused image were analyzed (Fig. 2e). A gray histogram can reflect the visual effect of the image. Through data analysis, the reflectance of Band 1 (blue) of Zhoushan aquaculture is between 48 and 2 979; for Band 2 (green), it ranges from 117 to 3 386; the reflectance of Band 3 (red) ranges from 29 to 3 499; for Band 4 (NIR), it ranges from –29 to 4022. The satellite gray histogram (Fig. 2e) shows that the gray histograms of Band 1 and Band 2 are more concentrated, and the contrast of ground object difference is poor. The wider the span of the transverse coordinates of Band 3 and Band 4 (Fig. 2e) is, it the more the difference between the water and aquaculture facility is. This means that Band 3 and Band 4, whose gray values are distributed more evenly, can better extract aquaculture information than Band 1 and Band 2 (Fig. 2e) (Lei et al., 2018). The mussel aquaculture area of Gouqi Island takes on a different tone in the four bands, Band 3 and Band 4 have larger grayscale ranges indicating more sensitivity to aquaculture areas.

In addition, to select sensitive bands of aquaculture area in the GF-6 satellite image, we compared the reflectance value of aquaculture floats and the water body nearby from the four bands in the image. First of all, one sampling point in the aquaculture floats area and one sampling point in the adjacent water body as a group was determined. Totally 20 groups of sampling points in this way were collected (Table 5) and the difference between the two sampling points in each group (that is the brightness difference between the floats area and the water body) was calculated. Finally, the average value of the differences for the 20 groups of data was obtained in one band. The difference values of the other three bands are obtained by the same method (Table 5). The larger the difference values of the band, the more sensitive the band is.

The water body and float pixel difference values of Band 1 and Band 2 are 120.35 and 126.45, being smaller than that of Band 3 and Band 4. It can be concluded that Band 3 and Band 4 in the GF-6 image are more sensitive than Band 1 and Band 2 in distinguishing mussel aquaculture areas from water bodies, with water body and float pixel difference values of 143.3 and 132.4, respectively. Therefore, the proportion of Band 3 and Band 4 can be appropriately increased in the process of aquaculture information extraction.

2.6.2 *Fishery ranching index*

According to the analysis above Band 3 and Band 4 of GF series satellite images are the sensitive bands of the Zhoushan mariculture area, and multiple information extraction models of the Zhoushan mariculture area are constructed (Cai et al., 2020).

Table 5. The water body and float pixel differences from Band 1 to Band 4

Group	Water body and float pixel difference			
	Band 1	Band 2	Band 3	Band 4
Group 1	60	50	47	113
Group 2	106	126	122	83
Group 3	249	249	228	199
Group 4	60	54	62	112
Group 5	69	70	108	145
Group 6	151	181	175	67
Group 7	88	93	107	98
Group 8	111	101	110	138
Group 9	146	124	104	129
Group 10	87	123	151	105
Group 11	51	52	66	89
Group 12	157	165	163	175
Group 13	85	85	103	139
Group 14	65	71	81	55
Group 15	87	70	102	150
Group 16	111	98	134	110
Group 17	162	161	182	132
Group 18	75	74	126	173
Group 19	269	316	318	184
Group 20	218	266	377	252
	120.35	**126.45**	**143.3**	**132.4**

Note: The bold numbers represent average values.

Then these models were compared with the traditional vegetation extraction index model Normalized Difference Vegetation Index (NDVI) (Wang et al., 2018) and water extraction index model Normalized Difference Water Index (NDWI) (Jiang and Ma, 2020). To get the extraction efficiency of these extraction algorithms, the extracted marine ranching area by every algorithm was verified using the same 230 marine ranching investigation points including 150 points aquacul cluding for the mussel farming area and 80 points aquacul cluding for the large yellow croaker farming area, obtained from July 25, 2020 and August 13, 2021, in the study area. According to the results of verification, the models with the best effect are selected as the fishery ranching index.

Based on preprocessed satellite images, enhancement was performed using radiation enhancement, spectral enhancement, and spatial domain enhancement. The aquaculture information was extracted using many different band combinations. Firstly, the band characteristics of phase satellite images are observed, and then continuous attempts are made to select the appropriate band for combination and calculation (Sarala and Jacob, 2014; Bai et al., 2021). A new method of Zhoushan aquaculture area extraction based on remote sensing can be obtained after continuous attempts and extracting effect comparison (Fig. 3). Finally, the following two models named fishery ranching index (FRI1 and FRI2, Eqs (9) and (10)) which are better for extracting aquaculture were proposed.

$$\mathrm{FRI1}:\ \ln\left|\mathrm{B4}-\frac{1}{2}\left(\mathrm{B3}+\frac{\mathrm{B1}+\mathrm{B2}}{2}\right)\right| / \ln\left|\mathrm{B4}+\frac{1}{2}\left(\mathrm{B3}+\frac{\mathrm{B1}+\mathrm{B2}}{2}\right)\right|, \tag{9}$$

$$\mathrm{FRI2}:\sqrt{\left|\frac{1}{2}\mathrm{B4}+\frac{1}{2}\left(\mathrm{B3}+\frac{\mathrm{B1}+\mathrm{B2}}{2}\right)\right|}, \tag{10}$$

where B1, B2, B3, and B4 are the values of Band 1, Band 2, Band 3, and Band 4 obtained from the GF-6 fusion image, respectively.

3 Results

3.1 *Zhoushan aquaculture area extraction*

In situ survey and the distribution of mussels and large yellow croaker, aquaculture areas are shown in Fig. 4. The fishery ranching index method was applied to distinguish the aquaculture area from ocean and land areas (Fig. 4). The mussel aquaculture information retrieved by using FRI is very clear, including the aquaculture area near Gouqi Island of 13 422 650.27 m^2 (Fig. 4a), and the large yellow croaker cage aquaculture area near Qingbang Island is 49 148 m^2 (Figs 4b and c). Hiding inside the island, the marine aquaculture area can obtain suitable water flow and shelter from wind shelter and protection from storm surges (typhoons), and other weather events.

The aquaculture is evenly distributed around the Gouqi Island and Qingbang Islands (Fig. 4) and mussel aquaculture areas are closely arranged by many similar rectangles with each cell of 102 × 50 m^2, with blocky distribution and rough texture characteristics, which can be well distinguished from the seawater (Fig. 4a). Meanwhile, large yellow croaker ranching areas are arranged by a lot of circular areas, with rough textures, which can be well distinguished from the seawater (Figs 4b and c).

Aquaculture areas can be distinguished from the surrounding waters sea and lands. Figures 4a, b and c are obtained by FRI1. This method can distinguish the mussel aquaculture area from the seawater and the island well in Fig. 4a except for the red circled area with high turbidity. Figures 4d, e and f are obtained from FRI2, can also distinguish the mussel aquaculture area from the seawater well as well as the red circled area, however bad in the green circled parts that are clearer in a1 extracted from FRI1 with low turbidity. FRI1 and FRI2 are complementary, and the combination of FRI1 and FRI2 is suitable for extracting mussel aquaculture areas. Figures 4e and f show that the result of FRI2 can not only separate the large yellow croaker ranching area from the seawater but also show the circle units. FRI2 plays a better role in extracting large yellow croaker aquaculture areas than FRI1 (Figs 4b and c).

$$\text{min}-\text{max normalization} = 255\ [(\mathrm{DN}-\mathrm{DN}_{\min})/(\mathrm{DN}_{\max}-\mathrm{DN}_{\min})]. \tag{11}$$

To verify the feasibility of the FRI , the extracted aquaculture area was verified using 52 aquaculture investigation points including 40 for the mussel aquaculture area and 12 for the large yellow croaker aquaculture area, obtained from July 25, 2020 and August 13 , 2021, in the study area. The verification method is as follows. The satellite image DN value after the FRI processing was

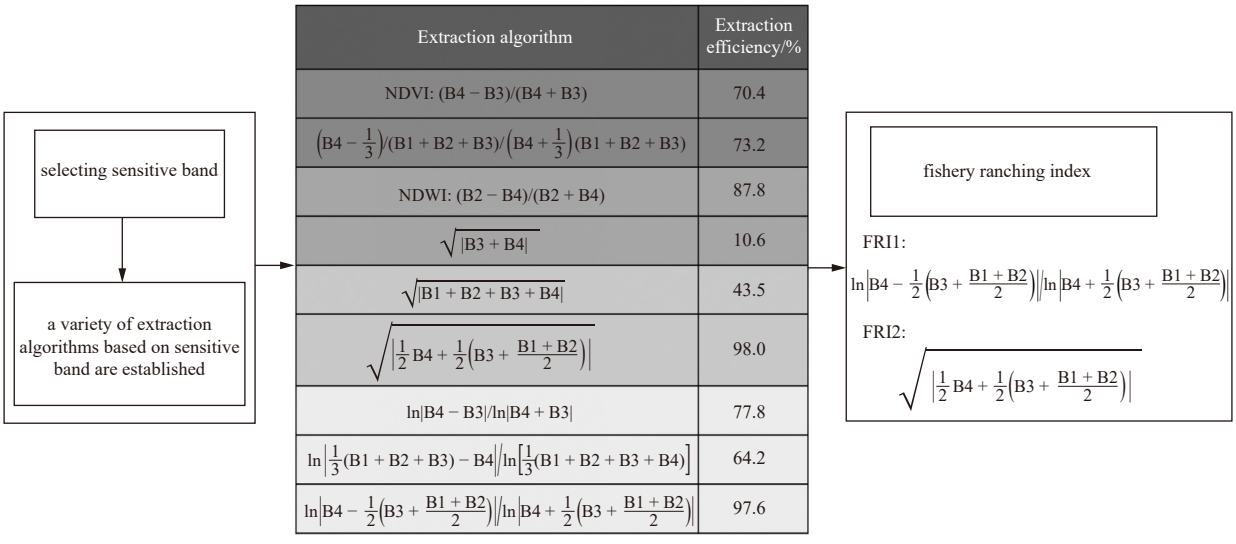

Fig. 3. Flow chart to determine fishery ranching index.

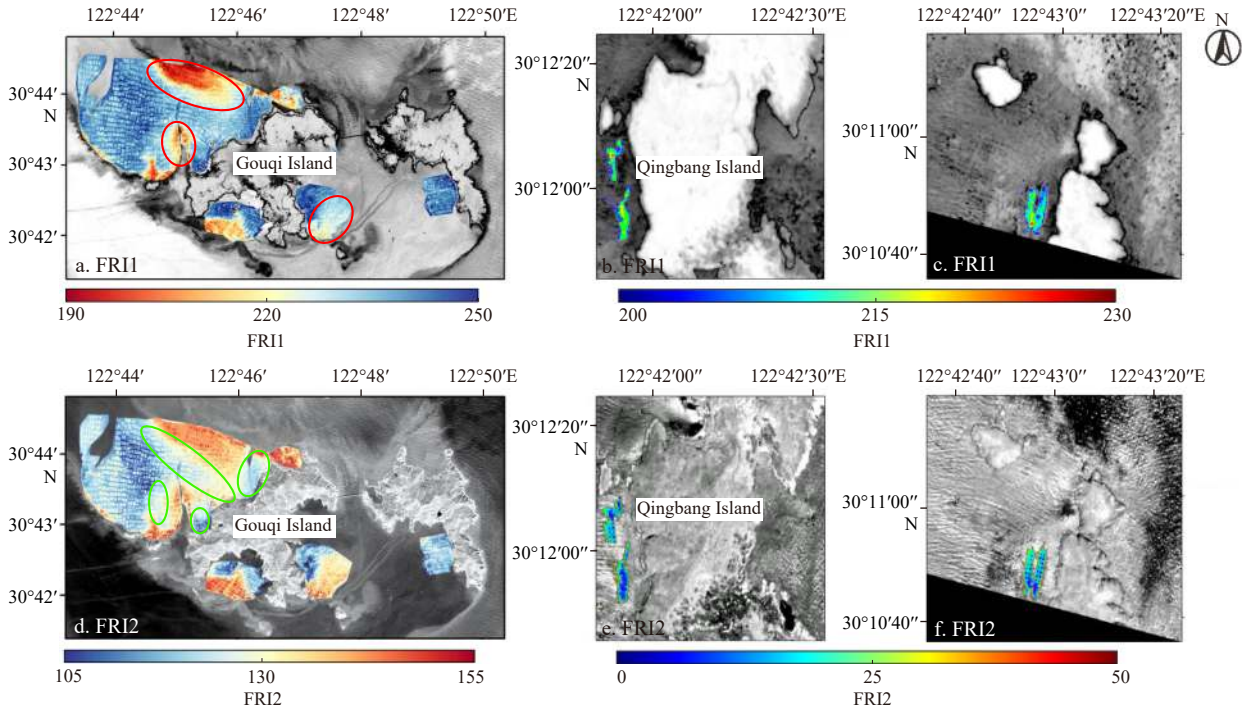

Fig. 4. Aquaculture area extracted using FRI1 (a, b, and c) and FRI2 (d, e, and f). The colorful parts in the image highlight the aquaculture area. Images in a and d are from GF-6 satelite data on October 3, 2019. Images in b, c, e, and f are from GF-6 satelite data on August 22, 2020. The colored parts in a and d are the main mussel aquaculture areas around Gouqi Island, and b, c, e, and f are large yellow croaker aquaculture areas around Dongji Qingbang Island.

transformed into the range of 0–255 by Eq. (11). One area with high sediment concentration and one area with low sediment concentration in the mussel aquaculture area near Gouqi Island of Zhoushan was selected, and the (ROI) regions of interest tool in ENVI software was used to randomly pick points from these two areas. Each group of point pairs consists of a floating raft point and its nearby water body points. DN difference value can be obtained by subtracting the DN values of the two points. The DN difference values are averaged to obtain the average value corresponding to different methods. Similarly, the operation was also carried out in the large yellow croaker aquaculture area near Qingbang Island in Zhoushan, and the results were as follows (Tables 6, 7, and 8).

In conclusion, the combination of FRI1 and FRI2 is more suit-

Table 6. Comparison of FRI in Gouqi Island mussel aquaculture area (high sediment concentration)

Group	FRI1 DN difference value	FRI2 DN difference value
Group 1	4.271 5	11.582 9
Group 2	1.142 1	7.874 9
Group 3	5.692 7	7.903 0
Group 4	1.280 1	3.981 9
Group 5	3.142 2	8.957 3
Group 6	1.252 1	6.189 2
Group 7	2.936 8	8.180 9
Group 8	4.943 5	11.482 1
Group 9	33.512 1	25.241 1
Group 10	15.915 1	17.154 8
	7.408 8	**10.854 8**

Note: The values in the table represent the water body and floating raft DN differences (from the FRI), and the bold numbers are average values. In the mussel aquaculture area with high sediment concentration, the difference between FRI2 sampling point pairs was greater than that of FRI1.

Table 7. Comparison of FRI in Gouqi Island mussel aquaculture area (low sediment concentration)

Group	FRI1 DN difference value	FRI2 DN difference value
Group 1	17.244 9	16.585 7
Group 2	16.988 5	18.643 9
Group 3	16.778 8	7.400 4
Group 4	12.705 2	10.159 9
Group 5	11.545 5	8.172 8
Group 6	10.093 3	9.144 8
Group 7	13.300 5	9.456 9
Group 8	12.543 0	8.631 5
Group 9	12.549 9	8.021 1
Group 10	14.536 9	6.851 2
	13.828 6	**10.306 8**

Note: The values in the table represent the water body and floating raft DN differences (from the FRI), and the bold numbers are average values. There was no significant difference between the FRI1 and FRI2 extraction in the mussel aquaculture area with low sediment concentration, but the difference between FRI1 sampling point pairs was still greater than that of FRI2.

Table 8. Comparison of FRI in Qingbang large yellow croaker aquaculture area

Group	FRI1 DN difference value	FRI2 DN difference value
Group 1	24.498 5	99.281 9
Group 2	6.948 3	197.278 1
Group 3	22.626 0	135.560 4
Group 4	54.208 2	119.973 8
Group 5	21.419 9	105.009 1
Group 6	21.423 3	152.374 4
	25.187 4	**134.913 0**

Note: The values in the table represent the water body and floating raft DN differences (from the FRI), and the bold numbers are average values. In the large yellow croaker aquaculture area, the difference of sampling point pairs by the FRI2 method was significantly larger than that by FRI1.

able for information extraction in mussel aquaculture areas. FRI1 is suitable for the mussel aquaculture area with low sediment concentration and FRI2 is suitable for the mussel aquaculture area with high sediment concentration. FRI2 is more suitable for information extraction in large yellow croaker cage aquaculture areas.

3.2 *Current and tide in Zhoushan aquaculture area*

The local tidal pattern is irregular semi-diurnal tide (Figs 5 and 6), and the velocity and direction change with time. Taking the current from August 29 to August 31, 2020 and December 13, 2020, as the example. According to the measured data of tidal flow (Fig. 5), the velocity and direction change with time. The tide rises and falls twice a day, and the tide range is asymmetric. During the flooding period, the current flows from east to west of Hangzhou Bay (Figs 6a and d). At ebb tide (Figs 6b, c, and e), the ebb tide flowing from the mouth of the Qiantang River to the east is divided into numerous small tidal currents as it passes over the Zhou Shan Islands, most of which flows to the southeast. The maximum surface flow velocity was 3.32 m/s, and the minimum flow velocity was 0.03 m/s. The maximum bottom flow velocity is

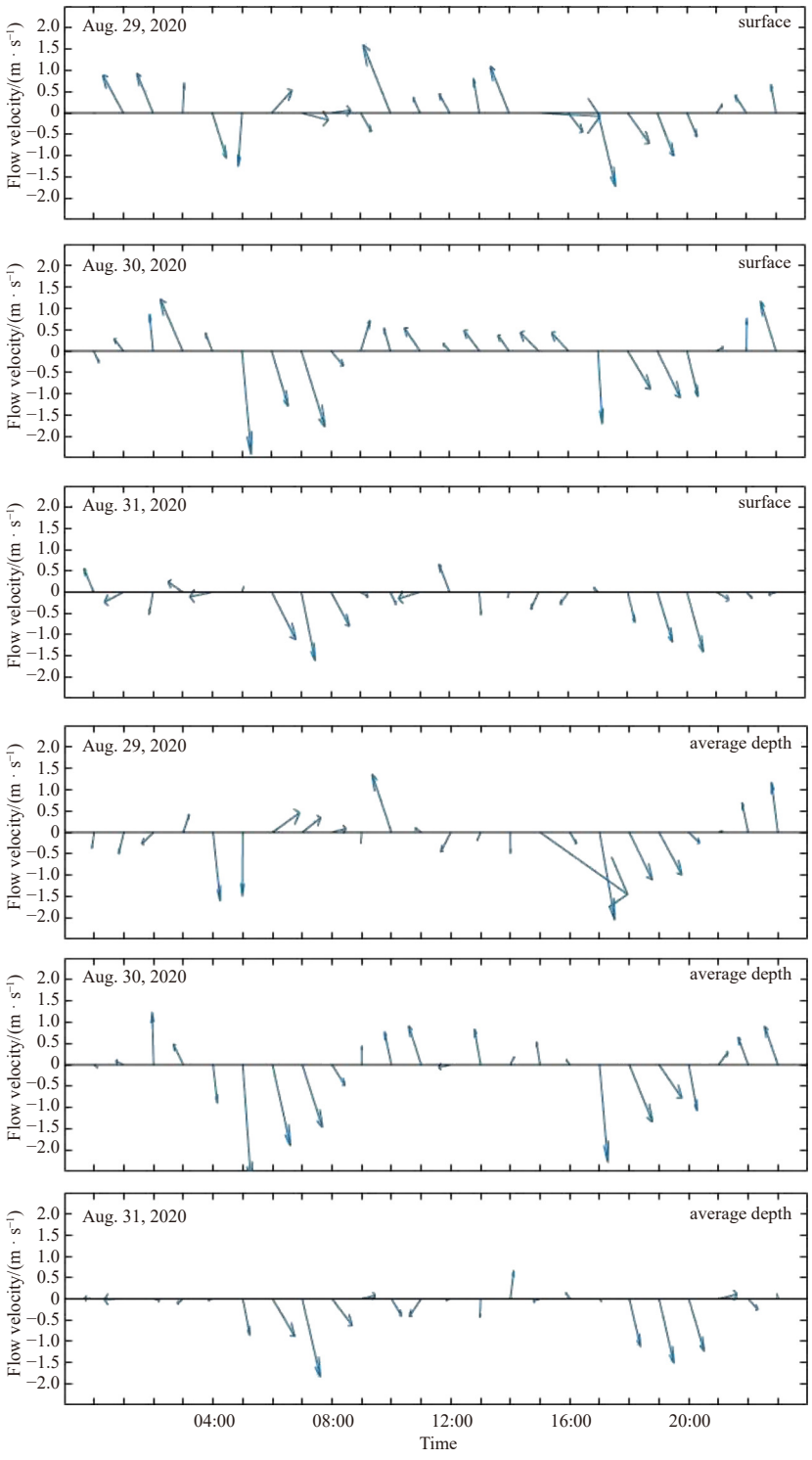

Fig. 5. Flow velocity and direction at surface and bottom during August 29 to August 31, 2020.

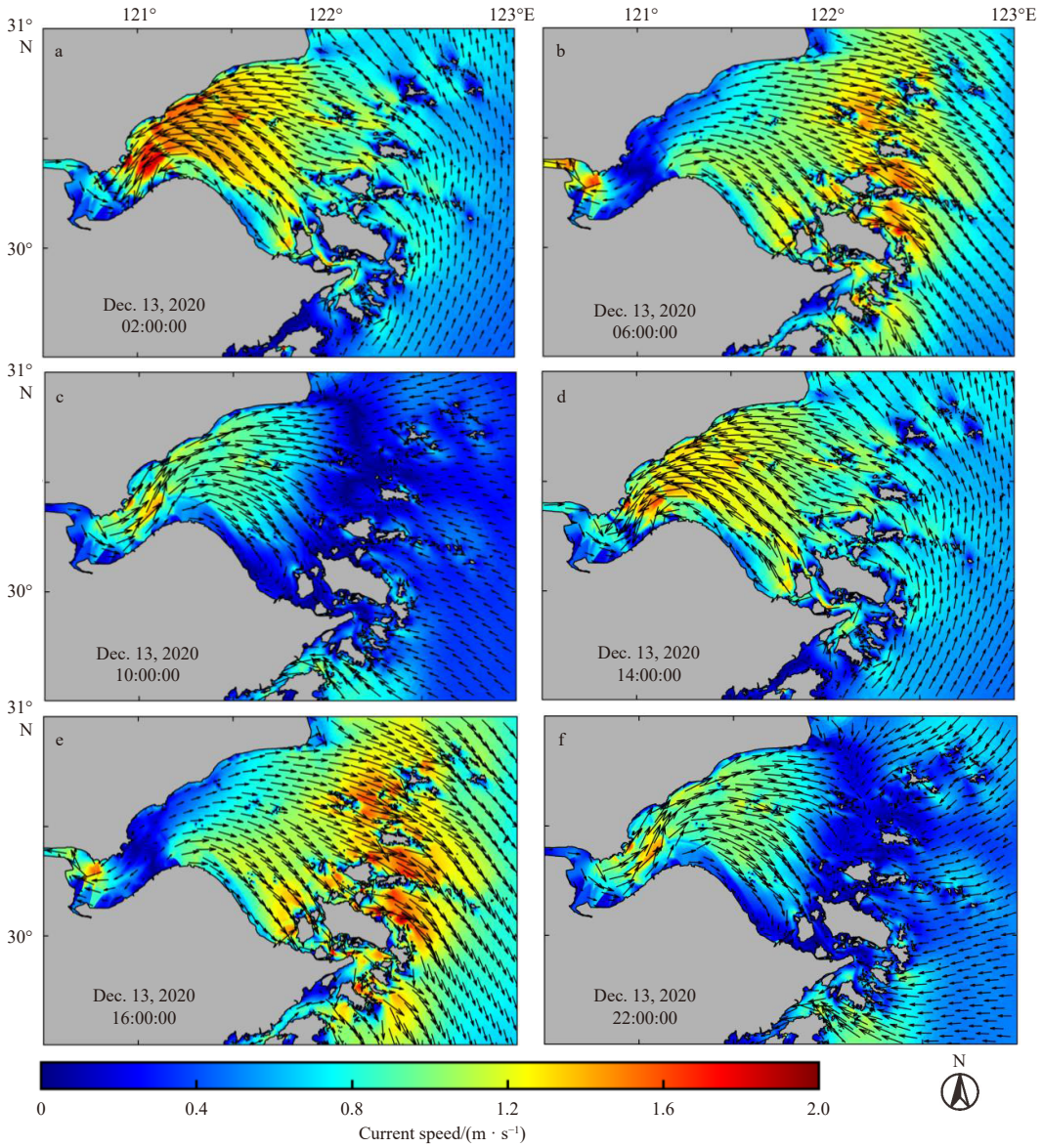

Fig. 6. The current of the Zhoushan sea area on December 13, 2020.

0.83 m/s, and the minimum bottom flow velocity is 0.17 m/s (Fig. 5). Tidal current interacts with islands forming upstream and downstream of the island. Tidal current influences the distribution of SSC, Chl-*a* concentration, SST, and other environmental factors.

3.3 *SST in Zhoushan aquaculture area*

SST near the mussel aquaculture area is generally in the range of 12–26℃ (Figs 7a–j), and 12–16℃ in winter (Figs 7b and j),and 22–26℃ in summer (Figs 7 d and e). SST near the large yellow croaker aquaculture area is mainly in the range of 12.6–26℃ (Figs 7a–j), and 12.6–18℃ in winter (Figs 7b and j), 22–26℃ in-summer (Figs 7d and e). There are also differences in SST in different months. The sea surface temperature in July, August, and September was higher, among which (Fig. 7e) the temperature in August in the study area was the highest, reaching 26℃. SST was low in December, March, and April, among which (Fig. 7b), the temperature in December in the study area was the lowest, only 12℃. The SST in winter is significantly lower than that in summer, and the difference between the two seasons is about 10℃. Islands influenced the SST, as the current interaction with islands induces the change of SST downstream of the island (Figs 7a–j). SST decreased downstream with the SST decreased by 1–4℃.

The characteristics of the SST distribution in the study area are closely related to the geographical location and climatic conditions of Zhoushan aquaculture. The optimum temperature provides good living conditions for marine organisms in the aquaculture area. Tidal currents interact with the island inducing turbulence downstream leading bottom waters and nutrients to the surface and providing a favorable condition for marine life to grow and develop.

3.4 *Chl-a distribution in the Zhoushan aquaculture area*

The concentration of Chl-*a* in the water near Zhoushan Islands is relatively high (Fig. 8), showing a decreasing trend from west to east (Fig. 8). The Chl-*a* concentration in the Zhoushan fishery is mainly in the range of 2–8 μg/L (Fig. 8) and the Chl-*a* concentration in the mussel aquaculture area ranges from 2–8 μg/L and large yellow croaker aquaculture area ranges from 3–9 μg/L (Fig. 8).

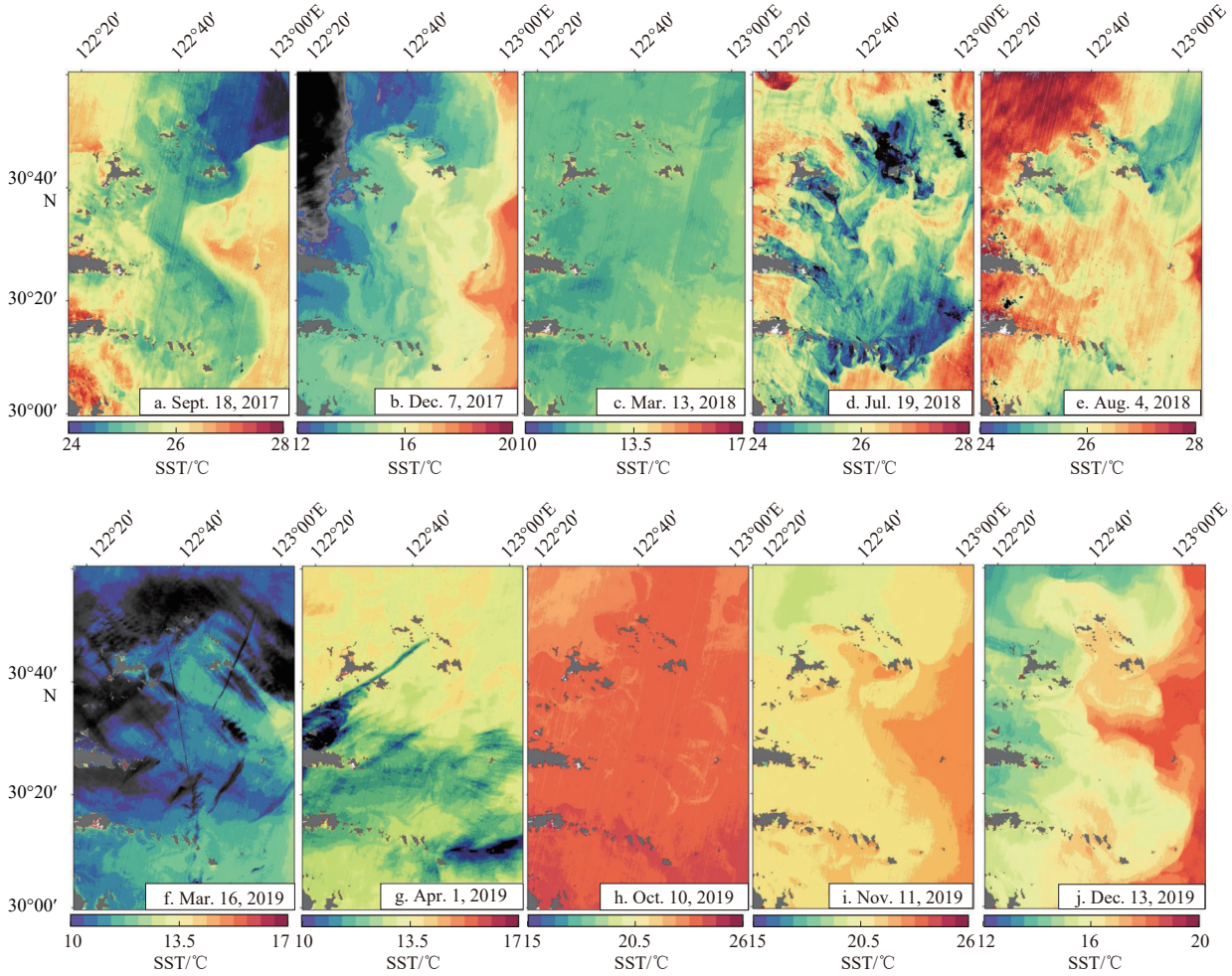

Fig. 7. SST retrieved from Landsat 8 TIRS image.

The spatial and temporal distribution of Chl-*a* concentration also has an obvious seasonal difference. The Chl-*a* concentration is about 1–5 μg/L in spring (Fig. 8s), 4–7 μg/L in summer (Fig. 8t), 5–8 μg/L in autumn (Fig. 8u), and 1–3 μg/L in winter (Fig. 8v), indicating that Chl-*a* concentration in Zhoushan aquaculture area decreased in the order of autumn, spring, summer, and winter (Figs 8s–v). Geographical location and season are two important factors affecting the chlorophyll distribution in the study area.

3.5 *SSC in Zhoushan aquaculture area*

The SSC of the mussel aquaculture area was 200–800 mg/L (Fig. 9), and that of the large yellow croaker aquaculture area was 250–600 mg/L (Fig. 9). SSC changes with the change of tidal current. Islands Interacting with tidal currents induce higher SSC downstream of islands than upstream with the SSC of 300–600 mg/L downstream and 200–400 mg/L upstream (Fig. 9). The distribution of SSC in Zhoushan sea surface was higher in winter (Figs 9 a, e, i, m, and o) and spring (Figs 9b, f, j, and n) than in summer (Figs 9c, g, and k) and autumn (Figs 9d, h, and l). Generally, SSC increases downstream, and a higher SSC belt can last about 10–15 km downstream (Fig. 9). Furthermore, it also shows a seasonal change due to seasonal factors such as the flood period and dry period. The concentration of SSC near Gouqi Island was about 500 mg/L in August and only about 250 mg/L in December.

3.6 *Other environmental factors in the Zhoushan aquaculture area*

Upwelling is common in the waters of Zhoushan. Figure 10 shows obvious upwelling in the study area (Fig. 10b). Upwelling appears in the Zhoushan Islands area in summer (Fig. 10b). The upwelling starts to form in spring it is obvious in summer. The upwelling begins to decline in the autumn and disappears completely in the winter. The upwelling brings abundant nutrients and food to the upper layer. Therefore, Zhoushan Islands have the natural advantage of being a marine aquaculture area.

Sea surface salinity (SSS) in the Zhoushan sea area is in the range of 20 to 30 (Figs 10e–h), and it increases from west to east, which is consistent with the characteristics of SSS increasing from nearshore to the ocean. SSS in spring and winter is about 25–30, which is slightly higher than that in summer and autumn (Fig.10f). Overall, the isohaline changes significantly at the mouth of the Changjiang River (Fig. 10f), indicating that Changjiang River Diluted Water has an impact on the salinity in summer. Changjiang River Diluted Water is the main reason for the seasonal variation of SSS in the Zhoushan sea area (Figs 10e–h). SSS value in the study area also provides suitable production conditions for marine organisms in the Zhoushan sea area.

The wind speed in the Zhoushan sea area is about 2 m/s in spring, 2–4 m/s in summer, 4–6 m/s in autumn, and 5-8 m/s in winter (Figs 10i–l). The wind direction is mainly southerly in summer and autumn and northerly in spring and winter. The change of wind field velocity and direction will affect the upwelling in the Zhoushan sea area and then affect the Chl-*a* con-

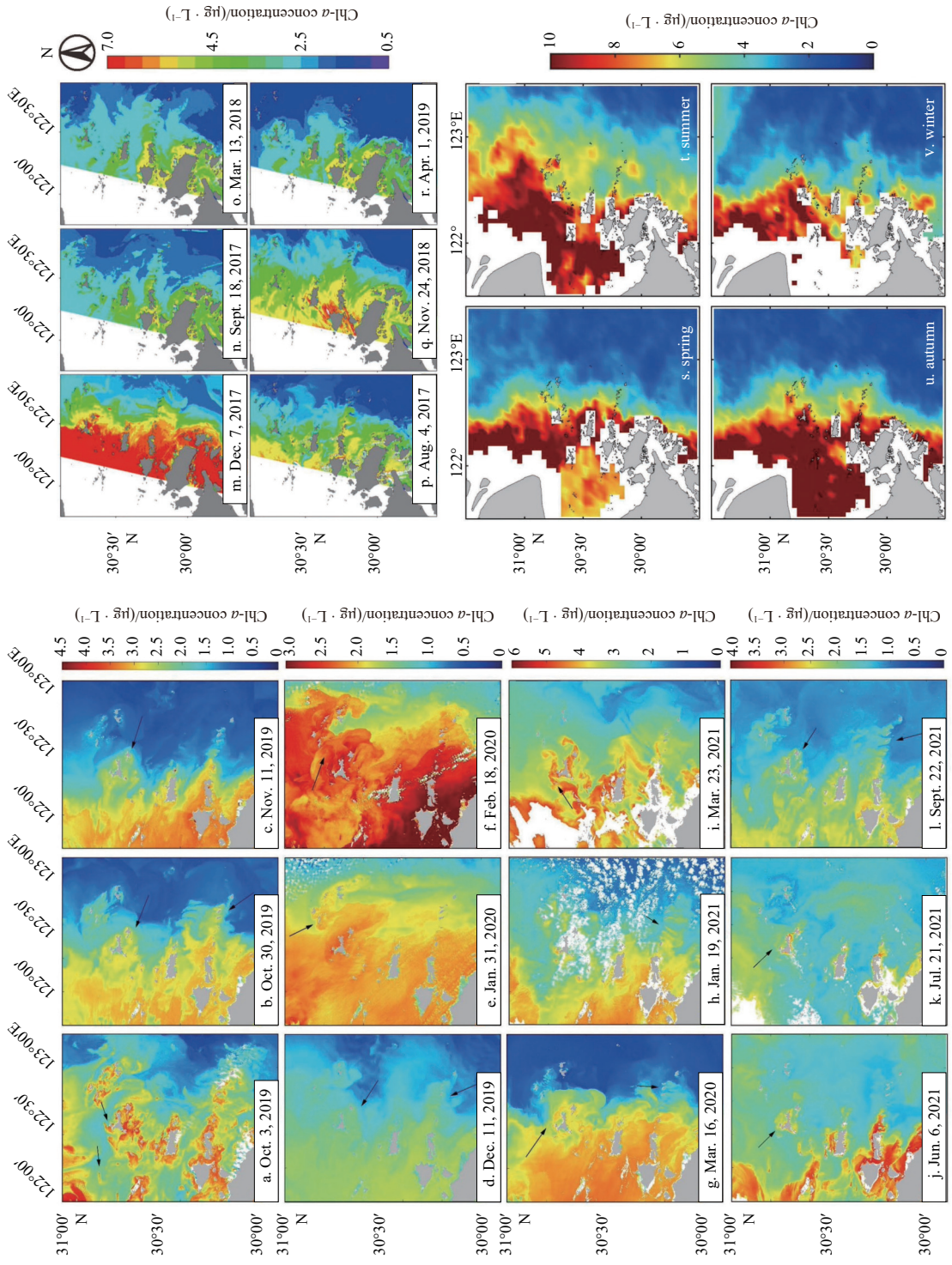

Fig. 8. Chl-*a* concentration distribution retrieved from HY-1C CZI images (a–l), Chl-*a* concentration distribution retrieved from Landsat8 images (m–r), and average Chl-*a* concentration distribution map from 2017 to 2020 (s–v). The black arrow indicates the direction of the local tidal current.

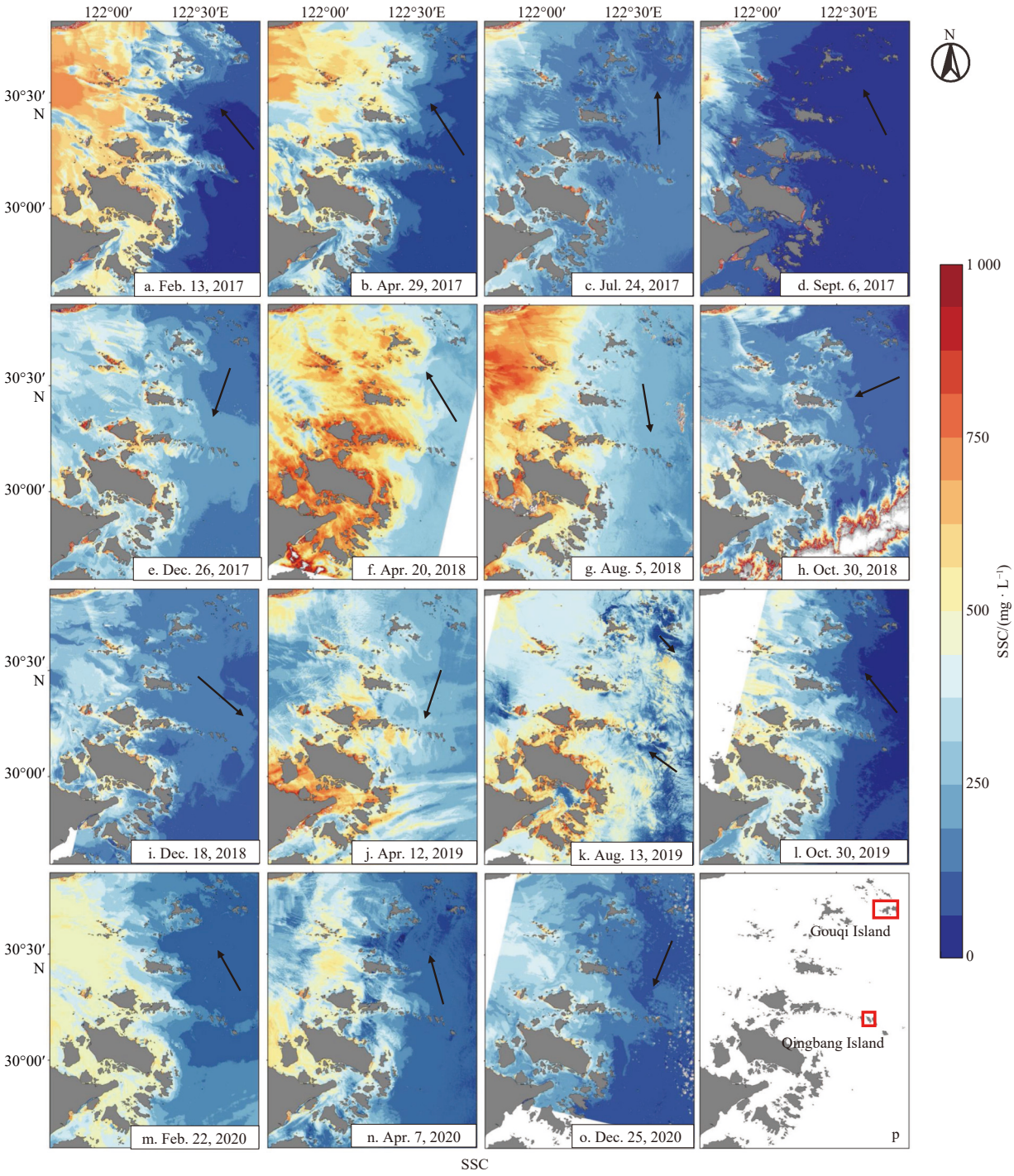

Fig. 9. SSC distribution in aquaculture area obtained from GF-1 wide field-of-view satellite images (a–o) and the study areas (p, red boxes). The black arrow indicates the direction of the tidal current.

centration distribution. Therefore, the wind also plays an important role in the contribution of the aquaculture area in Zhoushan.

4 Discussion

4.1 *The factors contributing to the formation of Zhoushan aquaculture*

There are three National Aquaculture Demonstration Zones in Zhoushan (Fig. 11), including the waters of the Zhongjieshan Islands area, the waters of the Ma'an Islands, and the Baisha sea area. Zhoushan aquaculture is generally distributed in the eastern part of the Zhoushan area and is dominated by the archipelago, far away from the mainland. Many factors, including SST, SSC, SSS, wind, current, and tide, and Chl-*a* concentration combined contribute to the development of aquaculture (Viúdez et al., 2016; Hu et al., 2021; Huo,1996).

4.1.1 *Suitable wind for the formation of aquaculture area*

The wind characteristics in the Zhoushan area show that the period from July to September Zhoushan area is dominated by tropical cyclones. This is also the important growth season for mussels and large yellow croaker. In addition, the location of

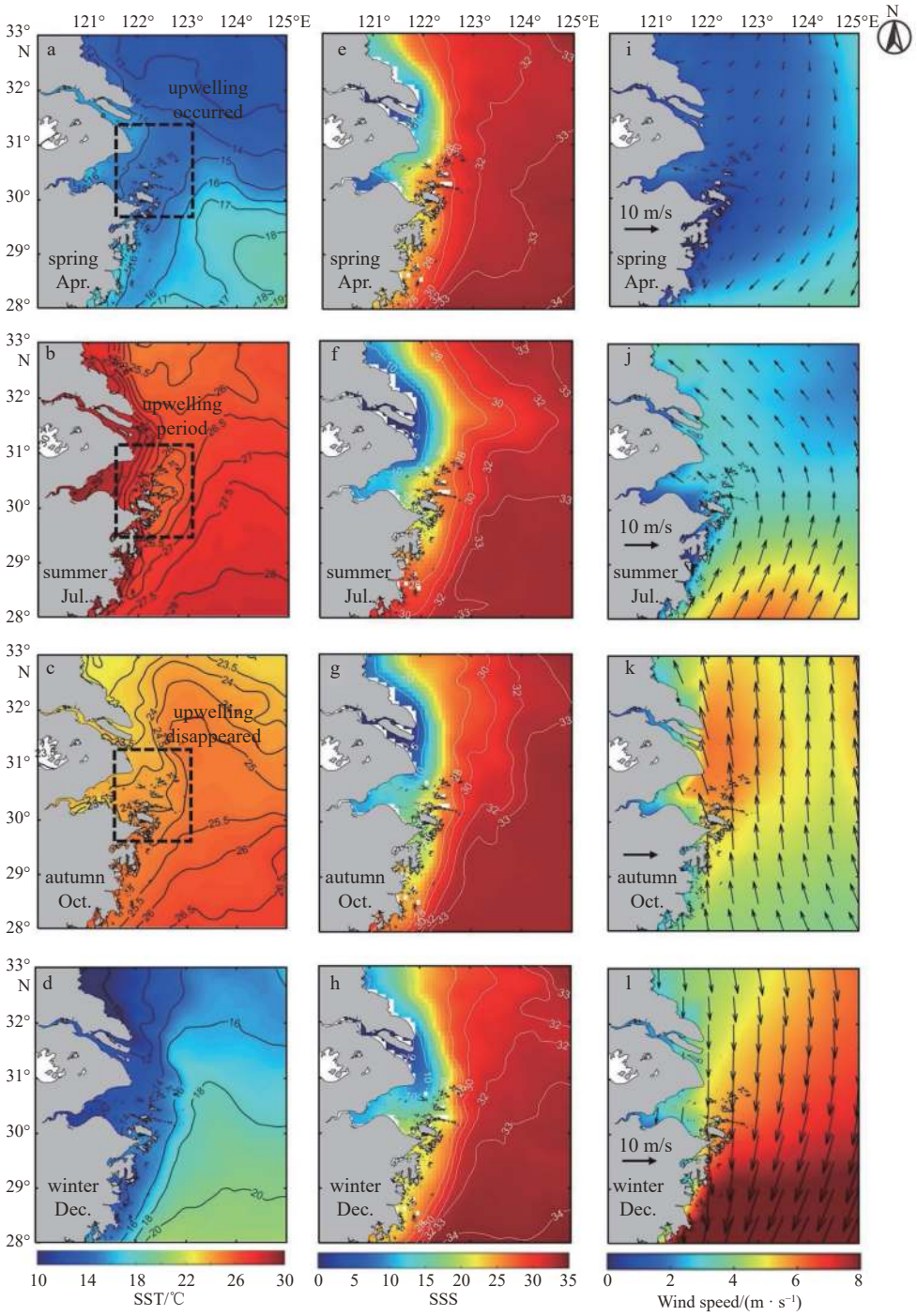

Fig. 10. The distribution of SST, SSS, and wind field. a b, c, and d were obtained from Group for High-Resolution SST (GHRSST) 2021 monthly mean SST data. e, f, g, and h were obtained from the 2021 SSS data provided by Copernicus Marine Environment Monitoring Service (CMEMS). i, j, k, and l were obtained from the 2021 monthly average wind field data provided by Pacific Islands Ocean Observing System (PacIOOS).

mussel and large yellow croaker aquaculture areas should not only be exposed but also be reasonably covered, and a balance should be found between exposing and covering. Because aquaculture areas need to be in the right open ocean to remove waste. At the same time, the aquaculture area should not be exposed to the open sea too much. Otherwise, there will be the risk of being damaged by wind and waves, thereby causing huge economic losses (Platt et al., 2015). In addition, the wind field in Zhoushan has obvious seasonal variations (Figs 10i–l), with the north wind prevailing in winter and the southeast wind prevailing in summer. The prevailing winds in summer induce the occurrence of offshore currents in the Zhoushan sea area, thus enhancing the upwelling so that the Zhoushan mussel and large yellow croaker aquaculture areas can obtain a lot of nutrients for the growth and development of mussels, large yellow croaker, and other organisms.

The Zhoushan sea area is vulnerable to typhoons. In 2004, a total of three typhoons landed in the Zhejiang Province of China, which also caused a huge impact on Zhoushan (Fig. 12a). The season of typhoons in the East China Sea is from July to Septem-

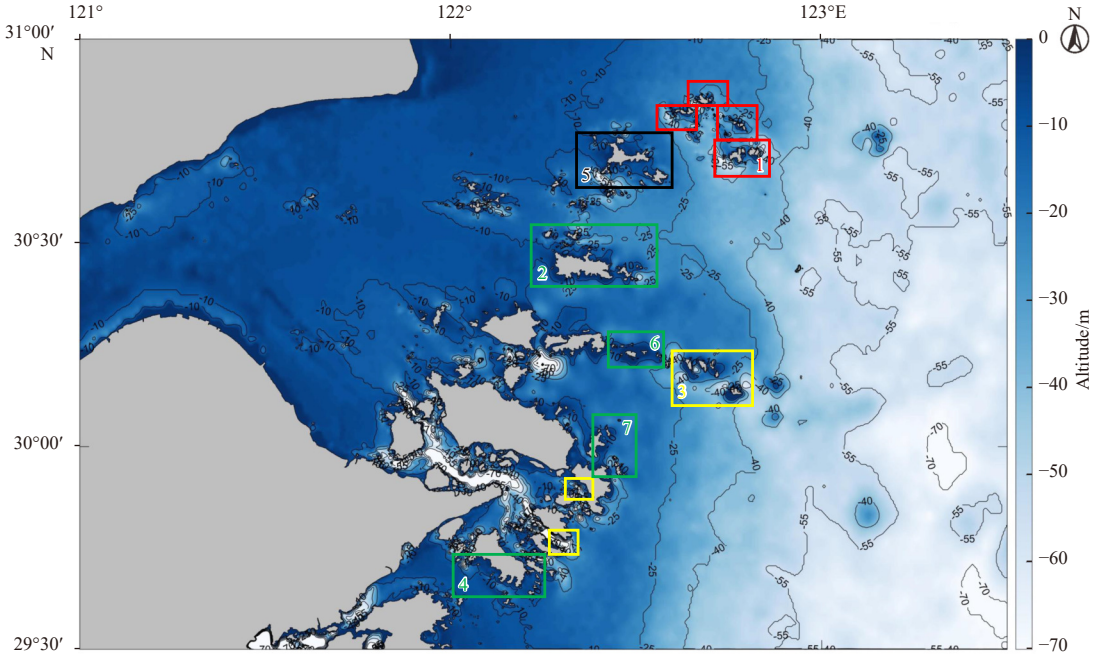

Fig. 11. Zhoushan mariculture area and potential mariculture area. The areas in the red boxes are mussel aquaculture area, the areas in the yellow boxes are large yellow croaker aquaculture area, the area in the black box is potential mussel aquaculture area and the areas in the green boxes are potential large yellow croaker aquaculture area. Areas 1, 2, 3, and 4 are the typical regions of the two aquaculture areas. Area 1: Gouqi Island area. Area 2: Qushan Islands area. Area 3: Qingbang Island area. Area 4: Liuheng Island area. Area 5: Shengsi Islands area. Area 6: Daxizhai Island area. Area 7: Putuo Mountain Island area.

ber every year, and August is the highest (Lu et al., 2018). The typhoon landing in Zhejiang Province also has a similar trend. The typhoon track that landed in Zhejiang since 1970 can be divided into three categories, among which the type of typhoon that landed in Zhejiang in the northwest direction has the greatest impact on the Zhoushan sea area, accounting for about 60%. This type of typhoon has the most serious impact on mussel and large yellow croaker aquaculture. Typhoon induces extremely heavy rain, with an average rainfall center of up to 199 mm (Dong and Huang, 2019). Typhoons often bring storm disasters, which will change the seawater environment of the aquaculture area and damage the aquaculture organisms in the aquaculture area. To reduce the impact of natural disasters on the aquaculture area, the suggestions should be considered as follows: (1) the location of the aquaculture area should be selected close to the island and away from the open sea side; (2) pay attention to short-term and long-term weather forecasts to reinforce their aquaculture areas before disasters; (3) after the disaster, the aquaculture area should be disinfected and repaired reasonably.

The mussel aquaculture area and large yellow croaker aquaculture area in Zhoushan are distributed in the upwelling area (Figs 10a–c). Upwelling can bring cold and nutrient-rich seawater from deep to the surface, which plays an important role in Chl-*a* concentration and marine productivity (Shafeeque et al., 2021). Determining the location of upwelling is crucial when locating potential marine ranches. Based on the temperature change brought by vertical seawater movement, it is found that there is obvious upwelling in Zhoushan in summer. The upwelling is formed by the combined effect of topography, Taiwan's warm current, and the southwest wind. Under the action of the southwest wind in summer, the surface seawater is transported offshore and the bottom seawater is compensated upward. This shows that wind plays a vital role in mussel and large yellow croaker aquaculture areas. Some researchers have also proposed the artificial construction of upwelling to use offshore wind energy for mariculture (Viúdez et al., 2016).

4.1.2 *Suitable temperature for the formation of aquaculture area*

SST is closely related to the temporal and spatial distribution of some marine economic fishes (Setiawati et al., 2015; Paulino et al., 2016; Apte et al., 2019; Ye et al., 2011; Xu et al., 2017). Setiawati et al. (2015) investigated the habitat of Thunnus Obesus using fishing data and environmental satellite data (SST, chlorophyll, sea surface height deviation) from the Java and Bali seas. Combined with Generalized Additive Model (GAM) statistical methods, Geographic Information System (GIS), satellite data, and recordings of fishery catch, prior researchers found that SST is the most important environmental variable to understand and predict the information on fishery resources. In addition, the relationship between the spatial distribution of Peruvian flying squid (Dosidicus Gigas) and SST as well as chlorophyll (Paulino et al., 2016)showed that the maximum catch was found in the SST between 18.4–22℃. Seasonal and interannual variations of SST help predict fishery distribution (Apte et al., 2019). From the literature on the appropriate temperature of mussels, it was known that all mussels died after 72 h of high temperature (Xu et al., 2017; Ye et al., 2011). The growth was slow in a low-temperature environment and could not be normal metamorphosis. The most suitable growth temperature for mussel is 20–25℃ (Ye et al., 2011). The most suitable growth temperature for large yellow crackers is 15–22℃ (Liu and De Mitcheson, 2008) which is consistent with the results in this study. The SST of Zhoushan mussel and large yellow croaker aquaculture areas remains between 12–16℃ in winter and 22–26℃ in summer (Fig. 7). The optimum temperature provides good living conditions for mussel aquaculture and large yellow croaker.

4.1.3 *Suitable tidal current for the formation of aquaculture area*

Tidal currents, bringing in large amounts of nutrient salts, in-

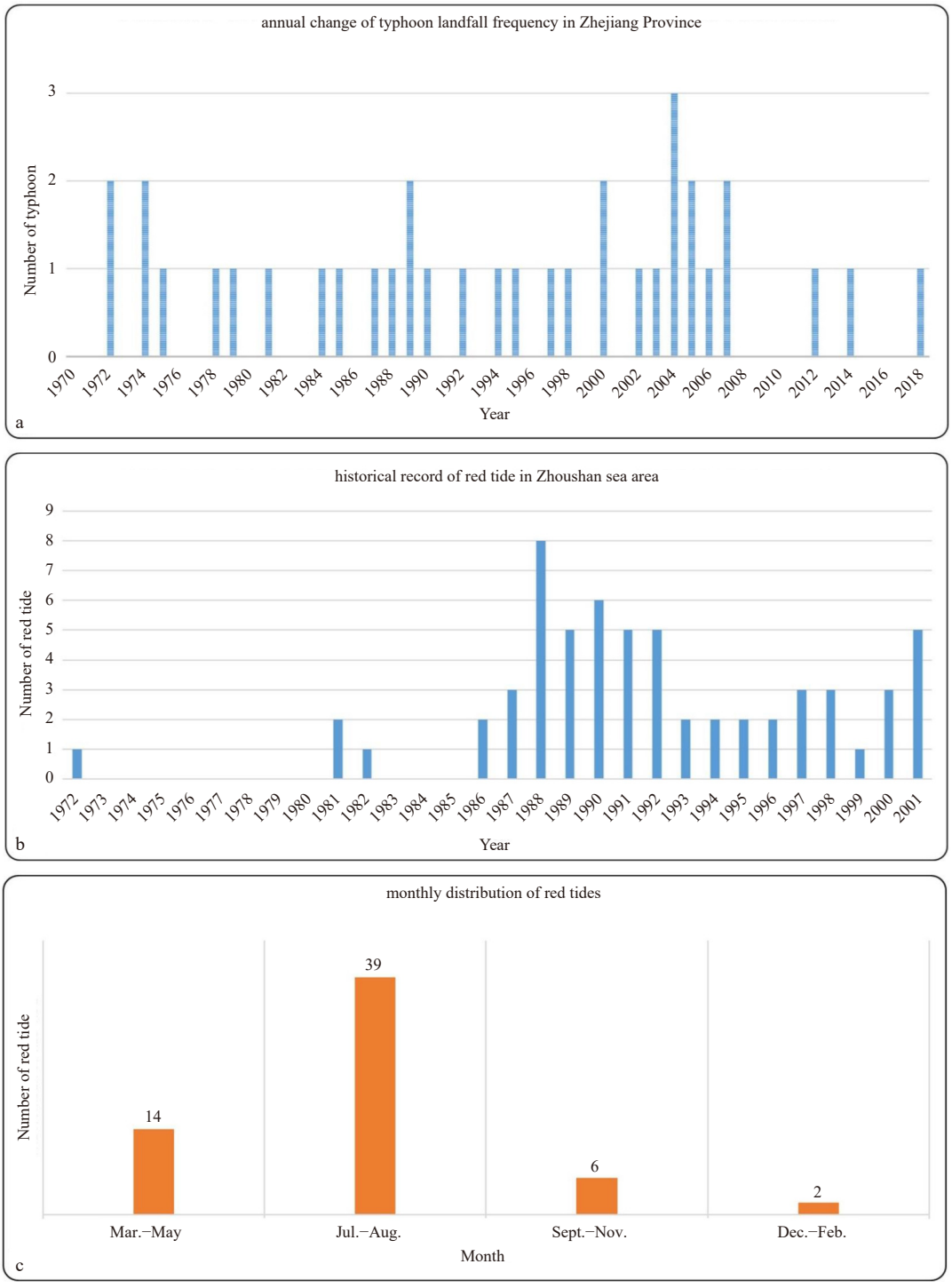

Fig. 12. Frequency of typhoons and red tides in the Zhoushan sea area.

ducing the change of phytoplankton, and many other fishery environmental factors (Chen et al., 2018b), have an important effect on fisheries. The world's largest fisheries lie at the confluence of warm and cold currents, or vertical compensating currents (Huo, 1996). Tidal current is necessary for the construction of aquaculture. The fish are easy to disperse to the outer sea or live in the upper middle under the effect of rapidly running water in the ocean. While the velocity of the small tidal current is slow, the fish are easy to concentrate on the inland sea and sink to the bottom, and it is a good opportunity for bottom trawler fishing (Yan et al., 2020). Therefore, to grasp the tide to determine the location of the fish area, net height, sailing time, and so on are important.

Zhoushan mussel and large yellow croaker aquaculture areas are mainly distributed in the area of dense islands. Meanwhile, regular currents provide favorable conditions for the development of marine life.

4.1.4 *Suitable Chl-a concentration and suspended sediment concentration for the formation of aquaculture area*

The Chl-*a* concentration and the abundance of plankton show a significant positive correlation. And plankton is closely re-

lated to Aquaculture areas. Chl-*a* concentration can reflect marine primary productivity (Platt et al., 2015). Marine primary productivity is the basis for the production of organic matter or economic products in the sea, as well as one of the important indicators to estimate the potential of marine productivity and fishery resources (Tan and Shi, 2006). In prior studies, the changes in estuarine physical and chemical properties through satellite data were analyzed and established a gradient with a close correlation between chlorophyll and SSC distribution (Miller and McKee, 2004), which further explained the effects of estuarine physical processes on organisms. A high SSC has an impact on water quality inducing the reduction of marine primary productivity near the estuary, and it is fatal to mussel and large yellow croaker aquaculture. Low marine primary productivity makes the growth of marine organisms slow or even die, which is very unfavorable for the large-scale and systematic cultivation of aquaculture.

The red tide occurs frequently from June to August (summer), followed by March to May (spring). The year with the highest number of red tides in the Zhoushan sea area was 1988, with a total of 8 red tides recorded (Figs 12b and c). The inversion of Chl-*a* concentration by remote sensing to predict the red tide bloom phenomenon can indicate that a high Chl-*a* concentration (Kimambo et al., 2019) is more prone to red tide and bloom (Platt et al., 2015). In addition, mussel and large yellow croaker along the coast accumulate toxicity due to “red tide”, which can easily lead to poisoning after eating.

Large yellow croaker is suitable for nearshore water, and the deterioration of water quality, such as red tide and eutrophication, will affect the growth of larva of large yellow croaker (Shikata et al., 2020). Excessive concentration of suspended substances will affect the primary productivity and then affect the organisms at all levels of the biological chain based on primary productivity (Wilkens et al., 2015), and then hurt the growth of large yellow croaker. Mussels are filter-feeding shellfish (Ye et al., 2011), and within a certain concentration range, the filtration rate and feeding rate of the shellfish increase with the increase of SSC. However, as the concentration of resuspension particles exceeds a certain concentration (Platt et al., 2015), the filtration rate, and feeding rate decrease rapidly, which is not conducive to the growth of mussels (Xu et al., 2017).

The concentration of Chl-*a* in the Zhoushan ranching area decreased from west to east and SSC in the study area ranged from 100 mg/L to 550 mg/L. It should be noted that the location where the SSC is not easy to accumulate is selected as the site selection for the aquaculture area (Torregroza-Espinosa et al., 2021). Suspend matter is also an important indicator to monitor whether the environment of mussel and large yellow croaker aquaculture areas is good. Excessively high SSC will worsen the water quality and the living conditions of marine organisms, thus affecting the construction and development of mussel and large yellow croaker aquaculture areas.

4.1.5 *Topographic feature*

Topographic features have an impact on the distribution of aquaculture areas (Tan and Shi, 2006). Taking Sections 3.2–3.5 as an example, it can be concluded that environmental factors such as SST and Chl-*a* concentration are related to the upstream and downstream locations of islands. Therefore, the comprehensive effect of islands and ocean currents should be taken into consideration when selecting the location for mussel and large yellow croaker aquaculture areas aquaculture. In addition, different Marine organisms have different preferences for seawater depth and seafloor sediments. For example, large yellow croaker in the East China Sea usually lives in the middle and lower layers of coastal and offshore waters within 80 m (Yu et al., 2022), and the depth of the spawning area is no more than 30 m. Large yellow croaker is more suitable to stay in the sediment and silty sediment during the winter (Yu et al., 2022). Therefore, we should also pay attention to the water depth, bottom quality, and other topographic features in the establishment of aquaculture areas.

4.2 *Potential aquaculture areas in Zhoushan*

There are many factors affecting mussel and large yellow croaker growth, and the environmental factors are complex (Tan and Shi, 2006; Miller and McKee, 2004). In addition to SST, Chl-*a* concentration, SSC, SSS, wind, and ocean current, some other environmental factors including oxygen content, Essential Fatty Acids (EFA), the dispersal of toxic metabolites and unconsumed food, cage damage by storms, transient water masses of temperature and oxygen content outside the tolerance range of the cultured species, the incidence of harmful algal blooms and so on could also be considered in the selection of the location of mussel aquaculture (Platt et al., 2015; Cheng et al., 2020). From the eye of a high special resolution optical satellite, we can obtain SST, Chl-*a* concentration as well as SSC as well as some ocean pollution that induces the change of water color. The factors obtained from the satellite in this study are only parts of the mussel production and large yellow croaker aquaculture environmental factors. Therefore, the mussel and large yellow croaker aquaculture area can be preliminarily screened out by using the two-step remote sensing method. Shengsi mussels began artificial aquaculture and gradually developed into a pillar industry, in 1973. As the main producing area of Shengsi mussels, Gouqi Island was named “Town of Mussels in Zhejiang Province” by the Zhejiang Marine Fisheries Bureau in 2001, and “Town of Mussels in China” by Zhoushan Fishery Association in 2010. Taking the mussel production in Shengsi in 2015 as an example, the mussel production in Gouqi Township accounted for 59% of the total output in Shengsi of Zhoushan. Because the parameters of environmental factors suitable for the survival and development of thick-shell mussels were highly consistent with the marine environmental factors of the mussel aquaculture area near Gouqi Island. Therefore, we take the environmental factors of the mussel aquaculture area around Gouqi Island as a reference. Globally, other waters, with similar environmental factors as the Gouqi Island mussel aquaculture area, will have the potential to develop an aquaculture area and can be developed as the site for the subsequent development of the mussel aquaculture area. According to the results of Section 3, we determined the water environment factor template suitable for mussel and large yellow croaker aquaculture.

Beyond satellite-observed factors, other relevant considerations, including the dispersal of toxic metabolites and unconsumed food (Platt et al., 2015); cage damage by storms (Platt

Table 9. Summary of marine environment factors in Zhoushan aquaculture areas

Area	SST/℃	SSC/ ($mg \cdot L^{-1}$)	SSS	Chl-*a* concentration/ ($\mu g \cdot L^{-1}$)	Current velocity/ ($m \cdot s^{-1}$)	Depth/m	Seafloor sediment	Upwelling
Zhoushan mussel aquaculture area	12–26	200–800	20–30	2–8	0.16–1.00	>15	silty clay	have
Zhoushan large yellow croaker aquaculture area	12.6–26	250–600	20–30	3–9	0.20–2.00	>17	oozy and silty clay	have

et al., 2015); transient water masses of temperature and oxygen content outside the tolerance range of the cultured species; and the incidence of harmful algal blooms (Platt et al., 2015; Nazeer and Nichol,2016; Wei et al., 2008)as well as the supply and demand of essential fatty acids, are essential in the aquaculture analysis. To accurately determine the location of potential mussel and large yellow croaker aquaculture areas, further judgment should be made in combination with these factors mentioned above in the next step.

Based on the study of SST, Chl-*a* concentration, ocean current, SSS, wind field, and SSC of Zhoushan aquaculture demonstration area (Table 9), the potential construction area of Zhoushan mussel aquaculture areas was found—Liuheng Town (Area 4 in Fig. 11). Liuheng Town, a port city, is the largest town in Zhoushan and has more than 100 islands. The environmental characteristics of the sea area near Liuheng Town are similar to those of the study area, with the average SST in summer around 24℃ and in winter around 15℃. SSC and Chl-*a* concentration were slightly higher than those in the study area. Therefore, crustaceans and shellfish can be mainly cultivated in this area.

In addition, Qushan Town (Area 2 in Fig. 11) is located in north-central Zhoushan, northeast of Daishan County, on the Changjiang River, Qiantang River estuary edge. In recent studies, it was also found to be the main growth, breeding, and fishing area of large yellow croaker, a specialty of Zhoushan. At the same time, the environmental characteristics of its nearby sea areas are similar to those of the study area in this paper. Therefore, Qushan Island can also be used as an area for Zhoushan to vigorously develop aquaculture for large yellow croakers in the future.

Statements such as the temperature range or local hydrodynamics or chlorophyll range matching the suitability requirements alone are not supportive enough to vividly describe these variables' relevance in the candidate species' life cycle. Therefore, in the preliminarily screened potential sites of the mussels and large yellow croaker aquaculture area aquaculture area, further selection should be conducted considering more environmental biochemical factors.

The remote sensing method, including two steps, was developed to help us locate potential mussels and large yellow croaker aquaculture areas. The first step is to determine the extraction model (FRI1 and FRI2) to extract the mussel and large yellow croaker aquaculture areas. FRI1 and FRI2 are complementary, and the combination of FRI1 and FRI2 is suitable for extracting mussel aquaculture areas. FRI2 is suitable for large yellow croaker aquaculture area extraction. This step is to reveal the location and spatial layout characteristics of the best mussel and large yellow croaker aquaculture areas. Gouqi mussel aquaculture area and Qingbang large yellow croaker aquaculture area are the most famous mussel and large yellow croaker aquaculture in China, with the best output and quality, and can be selected as a standard reference. The second step is analyzing the environmental factors obtained from satellite remote sensing data such as SST, Chl-*a* concentration, and SSC based on the extraction results. This step is to reveal the environmental characteristics of the best mussel and large yellow croaker aquaculture areas.

Based on the two-step-remote sensing method, satellite remote sensing technology can be used to determine the basic characteristics of the best mussel aquaculture area and large yellow croaker aquaculture area, including location layout and internal environmental factors. This two-step remote sensing method can be used for preliminary screening of potential aquaculture sites for mussels and large yellow croakers in other

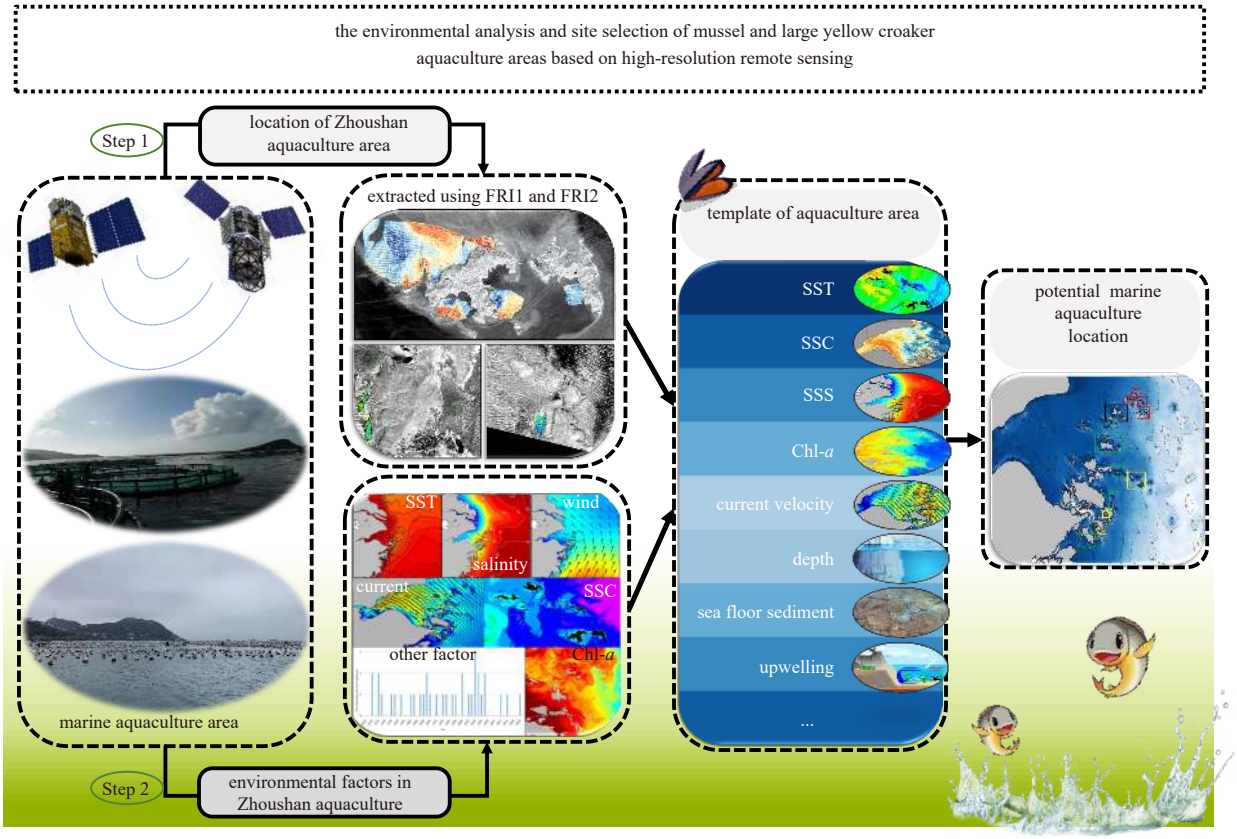

Fig. 13. Two-step remote sensing method and mechanism for potential site selection for the mussels and large yellow croaker aquaculture area.

areas.

Furthermore, the two-step method for determining potential aquaculture site selection, apart from applying to the site selection issue in potential aquaculture areas in Zhoushan, can also be employed for selecting sites in other similar aquatic regions for aquaculture. We also attempted to apply the same method in the coastal aquaculture area of Lianyungang City, Jiangsu Pro vince, China and achieved promising extraction results as well.

5 Conclusions

A new two-step remote sensing method was proposed and applied to analyze the basic environmental characteristics of the best mussel and large yellow croaker aquaculture areas. This methodology includes the first step of extraction of the location distribution and the second step of the extraction of internal environmental factors. During the first step stage, a new method fishery ranching index (FRI1, FRI2) was proposed to extract aquaculture using 2 m resolution fused data from GF-1 and GF-6. Mussel aquaculture areas and large yellow croaker aquaculture areas were extracted in detail. FRI 1 and FRI 2 are complementary, the combination of FRI1 and FRI2 is suitable to retrieve mussel aquaculture areas. FRI2 is suitable for extracting large yellow croaker aquaculture areas. Aquaculture (mussel aquaculture and large yellow croaker aquaculture area) in Zhoushan is mainly located on the side near the islands that are away from the eastern open waters. In the second step, the environmental factors of were extracted and analyzed (Fig. 13).

Based on the two-step remote sensing method, the environmental factor template for the mussel aquaculture area and the large yellow croaker aquaculture area were determined. The concentration of suspended matter in Zhoushan aquaculture area ranges from 200 mg/L to 800 mg/L, and the Chl-*a* concentration in the study area ranges from 2 μg/L to 9 μg/L. The interaction between the ocean currents and islands leads the SSC and Chl-*a* concentration to increase downstream of the islands. The SST in Zhoushan aquaculture sea area is between 12℃ and 26℃, and the SST downstream of the islands increases in winter and decreases in summer. The SSS of Zhoushan aquaculture is about 20–30. The flow velocity in Zhoushan mussel and large yellow croaker aquaculture area ranges from 0.16 m/s to 2.0 m/s.

According to the environmental characteristics of Zhoushan aquaculture, it can be found that the waters around Liuheng Island, Qushan Island, Putuo Mountain Island, and Daxizhai Island (Area 6 and Area 7 in Fig. 11) are suitable for large yellow croaker aquaculture, and Shengsi Islands (Area 5 in Fig. 11) are suitable for mussel aquaculture. Therefore, these sites can be potential Zhoushan aquaculture for development and utilization in the future.

This two-step remote sensing method can be applied for the preliminary screening of potential site selection for the mussels and large yellow croaker aquaculture area in the future (Fig. 13). The fishery ranching index (FRI1, FRI2) in this paper can be applied to extract the mussel and large yellow croaker aquaculture areas in other similar seas around the world.

Acknowledgements

HY-1C/D satellite data were provided by the National Satellite Ocean Application Service (NSOAS), Ministry of Natural Resources, China, obtained from the website: https://osdds.nsoas.org.cn (accessed on December 21, 2021). The authors would like to thank the NSOAS for providing the data free of charge. The authors thank the National Satellite Ocean Application Center, China, and the Sophisticated Ocean Front and Fisheries Investigation (SOPHI) for the data support.

References

Apte D, Narayana S, Dutta S. 2019. Impact of sea surface temperature anomalies on giant clam population dynamics in Lakshadweep reefs: inferences from a fourteen years study. Ecological Indicators, 107: 105604, doi: 10.1016/j.ecolind.2019.105604

Bai Zhaoguang. 2013. Technical characteristics of Gaofen-1 satellite. Aerospace China (in Chinese), 2013(8): 5–9

Bai Siqi, Zou Xiaorong, Zhang Peng, et al. 2021. Study on spatial heterogeneity effect of environmental factors on distribution of Chilean jack mackerel in Southeast Pacific Ocean. South China Fisheries Science (in Chinese), 17(1): 17–24, doi: 10.12131/20200172

Barsi J A, Schott J R, Hook S J, et al. 2014. Landsat-8 thermal infrared sensor (TIRS) vicarious radiometric calibration. Remote Sensing, 6(11): 11607–11626, doi: 10.3390/rs61111607

Blix K, Pálffy K, Tóth V R, et al. 2018. Remote sensing of water quality parameters over lake balaton by using Sentinel-3 OLCI. Water, 10(10): 1428, doi: 10.3390/w10101428

Cai Lina, Tang Rong, Yan Xiaojun, et al. 2022. The spatial-temporal consistency of chlorophyll-*a* and fishery resources in the water of the Zhoushan archipelago revealed by high resolution remote sensing. Frontiers in Marine Science, 9: 1022375, doi: 10.3389/fmars.2022.1022375

Cai Lina, Zhou Minrui, Liu Jianqiang, et al. 2020. HY-1C observations of the impacts of islands on suspended sediment distribution in Zhoushan coastal waters, China. Remote Sensing, 12(11): 1766, doi: 10.3390/rs12111766

Chang Jianbo. 1985. Japan builds new floating reef. Marine Fisheries (in Chinese), 1985(4): 191

Chen Fei. 2011. Research on industrialization development of large yellow croaker s cultivation in Zhejiang (in Chinese)[dissertation]. Zhoushan: Zhejiang Ocean University

Chen Peng, Chen Xinjun, Lei Lin. 2018b. Influence of Peruvian upwelling on the anchoveta (*Engraulis ringens*) fishing ground. Journal of Fisheries of China (in Chinese), 42(9): 1367–1377, doi: 10.11964/jfc.20170410806

Chen Hanyue, Zhu Li, Li Jiaguo, et al. 2018a. A comparison of two mono-window algorithms for retrieving sea surface temperature from Landsat8 data in coastal water of Hongyan River nuclear power station. Remote Sensing for Land & Resources (in Chinese), 30(1): 45–53, doi: 10.6046/gtzyyg.2018.01.07

Cheng K H, Chan S N, Lee J H W. 2020. Remote sensing of coastal algal blooms using unmanned aerial vehicles (UAVs). Marine Pollution Bulletin, 152: 110889, doi: 10.1016/j.marpolbul.2020.110889

Cheng Liang, Ma Youhua, Huang Yanyan, et al. 2011. Comparison of atmospheric correction between ENVI FLAASH and ERDAS ATCOR2. Agriculture Network Information (in Chinese), (12): 17–20, doi: 10.3969/j.issn.1672-6251.2011.12.006

Cui Xiaosong, Zhao Chenghai. 2005. Accuracy analysis of ADCP test in lake discharge test. Express Water Resources & Hydropower Information (in Chinese), 26(7): 18–20, doi: 10.15974/j.cnki.slsdkb.2005.07.005

De Mendonça J C, Lopes F B, De Andrade E M, et al. 2017. Monitoring water quality in a reservoir of the semi-arid region using remote sensing. Journal of Experimental Agriculture International, 19(1): 1–12, doi: 10.9734/JEAI/2017/37913

Dinguirard M, Slater P N. 1999. Calibration of space-multispectral imaging sensors: A review. Remote Sensing of Environment, 68(3): 194–205, doi: 10.1016/S0034-4257(98)00111-4

Dong Jiabin, Huang Xinqing. 2019. Typhoon track classification and rainstorm area analysis in Zhejiang. Journal of Zhejiang Meteorology (in Chinese), 40(3): 13–19, doi: 10.16000/j.cnki.zjqx.2019.03.003

Guo Han. 2018. HY-1C satellite. Satellite Application (in Chinese), (10): 66

Han Jiwei, Shao Jun, Fu Weii, et al. 2021b. ADCP velocity measurement by towing method based on micro-nano bubble tracer. Journal of China Hydrology (in Chinese), 41(2): 63–68, doi: 10.19797/j.cnki.1000-0852.20190306

Han Jie, Tao Zui, Xie Yong, et al. 2021a. A novel radiometric cross-

calibration of GF-6/WFV with MODIS at the dunhuang radiometric calibration site. IEEE Journal of Selected Topics in Applied Earth Observations and Remote Sensing, 14: 1645–1653, doi: 10.1109/JSTARS.2020.3046738

Hu Mingna. 2007. Coastal upwelling in the Zhoushan and its adjacent seas detected by satellite measurements (in Chinese)[dissertation]. Qingdao: Ocean University of China

Hu Jilian. 2020. Study on settlement velocity of near-shore suspended body in Zhoushan fishing ground. Rural Economy and Science-Technology (in Chinese), 31(3): 72–74,111, doi: 10.3969/j.issn.1007-7103.2020.03.033

Hu Qiwei, Chen Xiaoyan, Huang Wanyi, et al. 2021. Phytoplankton bloom triggered by eddy-wind interaction in the upwelling region East of Hainan Island. Journal of Marine Systems, 214: 103470, doi: 10.1016/j.jmarsys.2020.103470

Huang Lingguang, Fang Yu, Zhang Dawen, et al. 2016. Quantitative retrieval of chlorophyll a concentration based on Landsat-8 OLI in the lakes. Jiangxi Science (in Chinese), 34(4): 441–444,456, doi: 10.13990/j.issn1001-3679.2016.04.009

Huo Fuhuai. 1996. Four major fishing grounds in the world. Journal of Educational Studies (in Chinese), (6): 39

Jia Kun, Liang Shunlin, Gu Xingfa, et al. 2016. Fractional vegetation cover estimation algorithm for Chinese GF-1 wide field view data. Remote Sensing of Environment, 177: 184–191, doi: 10.1016/j.rse.2016.02.019

Jiang Zongchen, Ma Yi. 2020. Accurate extraction of offshore raft aquaculture areas based on a 3D-CNN model. International Journal of Remote Sensing, 41(14): 5457–5481, doi: 10.1080/01431161.2020.1737340

Kimambo O N, Chikoore H, Gumbo J R, et al. 2019. Retrospective analysis of Chlorophyll-*a* and its correlation with climate and hydrological variations in Mindu Dam, Morogoro, Tanzania. Heliyon, 5(11): e02834, doi: 10.1016/j.heliyon.2019.e02834

Lei Sen, Zou Zhengxia, Liu Dunge, et al. 2018. Sea-land segmentation for infrared remote sensing images based on superpixels and multi-scale features. Infrared Physics & Technology, 91: 12–17, doi: 10.1016/j.infrared.2018.03.012

Li Siyuan, He Zhijiang, Yu Hongyue, et al. 2021a. Comparative study on microbial community in mussel *mytilus coruscus* body and seawater of its natural and cultural sea area in Zhoushan, Zhejiang. Oceanologia et Limnologia Sinica (in Chinese), 52(1): 196–205, doi: 10.11693/hyhz20200700217

Li Yan, Shang Shaoling, Zhang Caiyun, et al. 2006. Remote sensing of algal blooms using a turbidity-free function for near-infrared and red signals. Chinese Science Bulletin, 51(4): 464–471, doi: 10.1007/s11434-006-0464-2

Li Liwei, Wang Wei, Wu Xuejiao. 2019. Study on orthorectification and image fusion algorithm of GF-1 satellite imagery in forest resource extraction. Journal of Green Science and Technology (in Chinese), (8): 219–222, doi: 10.16663/j.cnki.lskj.2019.08.079

Li Xiaoyu, Yu Rencheng, Geng Huixia, et al. 2021b. Increasing dominance of dinoflagellate red tides in the coastal waters of Yellow Sea, China. Marine Pollution Bulletin, 168: 112439, doi: 10.1016/J.MARPOLBUL.2021.112439

Liang Xiaoxia. 2018. Long March 2C carrier rocket successfully launched HY-1C satellite. Missiles and Space Vehicles (in Chinese), (5): 56

Liu Min, De Mitcheson Y S. 2008. Profile of a fishery collapse: why mariculture failed to save the large yellow croaker. Fish and Fisheries, 9(3): 219–242, doi: 10.1111/j.1467-2979.2008.00278.x

Loveland T R, Irons J R. 2016. Landsat 8: the plans, the reality, and the legacy. Remote Sensing of Environment, 185: 1–6, doi: 10.1016/j.rse.2016.07.033

Lu Xiaojie, Dong Changming, Li Gang. 2018. Variations of typhoon frequency and landfall position in East China Sea from 1951 to 2015. Transactions of Atmospheric Sciences (in Chinese), 41(4): 433–440, doi: 10.13878/j.cnki.dqkxxb.20170803001

Ma Yichao, Mi Hongyan, Zhong Kai. 2018. Research on urban ecological environment of high resolution remote sensing image based on ENVI. Computer Engineering & Software (in Chinese), 39(11): 235–238, doi: 10.3969/j.issn.1003-6970.2018.11.049

Ma Junying, Yang Jiming. 1994. Marine ranch studies in Japan. Marine Sciences (in Chinese), (3): 23–24

Massarelli C, Galeone C, Savino I, et al. 2021. Towards sustainable management of mussel farming through high-resolution images and open source software-the taranto case study. Remote Sensing, 13(15): 2985, doi: 10.3390/rs13152985

Miller R L, McKee B A. 2004. Using MODIS Terra 250 m imagery to map concentrations of total suspended matter in coastal waters. Remote Sensing of Environment, 93(1-2): 259–266, doi: 10.1016/j.rse.2004.07.012

Nazeer M, Nichol J E. 2016. Development and application of a remote sensing-based Chlorophyll-*a* concentration prediction model for complex coastal waters of Hong Kong. Journal of Hydrology, 532: 80–89, doi: 10.1016/j.jhydrol.2015.11.037

Ottinger M, Clauss K, Kuenzer C. 2017. Large-scale assessment of coastal aquaculture ponds with Sentinel-1 time series data. Remote Sensing, 9(5): 440, doi: 10.3390/rs9050440

Paulino C, Segura M, Chacón G. 2016. Spatial variability of jumbo flying squid (*Dosidicus gigas*) fishery related to remotely sensed SST and chlorophyll-*a* concentration (2004–2012). Fisheries Research, 173: 122–127, doi: 10.1016/j.fishres.2015.10.006

Perkins S. 2019. Inner workings: ramping up the fight against Florida's red tides. Proceedings of the National Academy of Sciences of the United States of America, 116(14): 6510–6512, doi: 10.1073/pnas.1902219116

Platt T, Shah P, George G, et al. 2015. Use of remote sensing in the context of cage aquaculture. In: Proceedings of the 5th International Symposium on Cage Aquaculture in Asia. Kochi, India: CMFRI and Asian Fisheries Society Qin Zhihao, Karnieli A. 1999. Progress in the remote sensing of land surface temperature and ground emissivity using NOAA-AVHRR data. International Journal of Remote Sensing, 20(12): 2367–2393, doi: 10.1080/014311699212074

Qin Zhihao, Karnieli A, Berliner P. 2001. A mono-window algorithm for retrieving land surface temperature from Landsat TM data and its application to the Israel-Egypt border region. International Journal of Remote Sensing, 22(18): 3719–3746, doi: 10.1080/01431160010006971

Reporter. 2020. Implement the guiding principles of the fifth Plenary Session of the 19th CPC Central Committee. People's Daily (in Chinese), 2020-11-12, doi: 10.28655/n.cnki.nrmrb.2020.011245

Roy D P, Wulder M A, Loveland T R, et al. 2014. Landsat-8: science and product vision for terrestrial global change research. Remote Sensing of Environment, 145: 154–172, doi: 10.1016/j.rse.2014.02.001

Sarala D, Jacob S. 2014. Digital image processing—A remote sensing perspective. International Journal of Innovative Research and Development, 3(12): 295–300

Setiawati M D, Sambah A B, Miura F, et al. 2015. Characterization of bigeye tuna habitat in the southern waters off Java–Bali using remote sensing data. Advances in Space Research, 55(2): 732–746, doi: 10.1016/j.asr.2014.10.007

Shafeeque M, Balchand A N, Shah P, et al. 2021. Spatio-temporal variability of chlorophyll-*a* in response to coastal upwelling and mesoscale eddies in the south eastern Arabian Sea. International Journal of Remote Sensing, 42(13): 4836–4863, doi: 10.1080/01431161.2021.1899329

Shikata T, Taniguchi E, Sakamoto S, et al. 2020. Phylogeny, growth and toxicity of the noxious red-tide dinoflagellate *Alexandrium leei* in Japan. Regional Studies in Marine Science, 36: 101265, doi: 10.1016/j.rsma.2020.101265

Song Yaming. 2001. Hydrological characteristics of Zhoushan Islands. Journal of China Hydrology (in Chinese), 21(6): 59–62, doi: 10.3969/j.issn.1000-0852.2001.06.019

Sui Baikai, Jiang Tao, Zhang Zhen, et al. 2020. A modeling method for automatic extraction of offshore aquaculture zones based on semantic segmentation. ISPRS International Journal of Geo-Information, 9(3): 145, doi: 10.3390/ijgi9030145

Sun Jun. 2005. Zeng Chengkui: life as a marine scientist. China Education Daily (in Chinese), 2005-03-24

Sun Pan, Dong Yusen, Chen Weitao, et al. 2016. Research on fusion

of GF-2 imagery and quality evaluation. Remote Sensing for Natural Resources (in Chinese), 28(4): 108–113, doi: 10.6046/gtzyyg.2016.04.17

Tan Saichun, Shi Guangyu. 2006. Remote sensing for ocean primary productivity and its spatio-temporal variability in the China Seas. Acta Geographica Sinica (in Chinese), 61(11): 1189–1199, doi: 10.3321/j.issn:0375-5444.2006.11.008

Teng Yue, Zou Bin, Ye Xiaomin. 2022. Study on the chlorophyll *a* concentration retrieved from HY-1C satellite coastal zone imager data. Haiyang Xuebao (in Chinese), 44(5): 25–34

Torregroza-Espinosa A C, Restrepo J C, Escobar J, et al. 2021. Spatial and temporal variability of temperature, salinity and chlorophyll-*a* in the Magdalena River mouth, Caribbean Sea. Journal of South American Earth Sciences, 105: 102978, doi: 10.1016/j.jsames.2020.102978

Viúdez Á, Balsells M F P, Rodríguez-Marroyo R. 2016. Artificial upwelling using offshore wind energy for mariculture applications. Scientia Marina, 80(S1): 235–248, doi: 10.3989/scimar.04297.06B

Wang Xu. 2018. A LM-2D carrier rocket successfully sends GF-6 satellite into orbit. Aerospace China (in Chinese), (6): 14, doi: 10.3969/j.issn.1002-7742.2018.06.004

Wang Fei, Qin Zhihao, Song Caiying, et al. 2015. An improved mono-window algorithm for land surface temperature retrieval from Landsat 8 thermal infrared sensor data. Remote Sensing, 7(4): 4268–4289, doi: 10.3390/rs70404268

Wang Zhihua, Yang Xiaomei, Liu Yueming, et al. 2018. Extraction of coastal raft cultivation area with heterogeneous water background by thresholding object-based visually salient NDVI from high spatial resolution imagery. Remote Sensing Letters, 9(9): 839–846, doi: 10.1080/2150704X.2018.1468103

Wang Wei, Yang Fang, Zhang Peng, et al. 2020. An approach for automatic preprocessing of high-resolution remote sensing data and vegetation extraction based on ENVI/IDL: a case study of hunan forestry. Journal of Hunan City University (Natural Science)(in Chinese), 29(2): 45–50, doi: 10.3969/j.issn.1672-7304.2020.02.0012

Wei Guifeng, Tang Danling, Wang Sufen. 2008. Distribution of chlorophyll and harmful algal blooms (HABs): a review on space based studies in the coastal environments of Chinese marginal seas. Advances in Space Research, 41(1): 12–19, doi: 10.1016/j.asr.2007.01.037

Wilkens J L, Katzenmeyer A W, Hahn N M, et al. 2015. Laboratory test of suspended sediment effects on short-term survival and swimming performance of juvenile Atlantic sturgeon (*Acipenser oxyrinchus oxyrinchus*, Mitchill, 1815). Journal of Applied Ichthyology, 31(6): 984–990, doi: 10.1111/jai.12875

Wong W H, Levinton J S. 2004. Culture of the blue mussel *Mytilus edulis* (Linnaeus, 1758) fed both phytoplankton and zooplankton: a microcosm experiment. Aquaculture Research, 35(10): 965–969, doi: 10.1111/j.1365-2109.2004.01107.x

Xu Hanqiu. 2015. Retrieval of the reflectance and land surface temperature of the newly-launched Landsat 8 satellite. Chinese Journal of Geophysics (in Chinese), 58(3): 741–747, doi: 10.6038/cjg20150304

Xu Jiakang, Peng Lihua, Gao Wei, et al. 2017. Effects of light intensity, water temperature and density on aggregation of juvenile mussel *Mytilus coruscus*. Journal of Dalian Ocean University (in Chinese), 32(3): 275–279, doi: 10.16535/j.cnki.dlhyxb.2017.03.004

Yan Hua, Chen Ying. 2021. Analysis of relative radiometric correction method for GF-6 satellite. Science & Technology Vision (in Chinese), (3): 5–8, doi: 10.19694/j.cnki.issn2095-2457.2021.03.02

Yan Mingjun, Hu Chunting, Lin Danging, et al. 2020. The diversity of fish communities and the effects of tidal intensity in the nearshore lower reaches of Yangtze River. Chinese Journal of Ecology (in Chinese), 39(6): 1865–1874, doi: 10.13292/j.1000-4890.202006.030

Yang Long. 2020. ENVI high-resolution remote sensing image data preprocessing. Journal of Jiaozuo University (in Chinese), 34(1): 97–100, doi: 10.16214/j.cnki.cn41-1276/g4.2020.01.022

Yang Hongsheng, Huo Da, Xu Qiang. 2016. Views on modern marine ranching. Oceanologia et Limnologia Sinica (in Chinese), 47(6): 1059–1074, doi: 10.11693/hyhz20160900203

Yang Xianping, Sokoletsky L, Hui Wu. 2017. Water quality seasonal variability (2000 to 2015) in Yangtze River estuary and its adjacent coastal area. Journal of Remote Sensing & GIS, 6(4): 1000216

Yang Yipeng, Wang Qiao, Xiao Qing, et al. 2006. Quantitative remote sensing inversion methods of chlorophyll-*a* concentration in Taihu Lake based on TM data. Geography and Geo-Information Science, 22(2): 5–8, doi: 10.3969/j.issn.1672-0504.2006.02.002

Yang Hongsheng, Zhou Yi. 1998. Research progress on the effects of filter-feeding shellfish on the environment of cultured Marine areas. Marine Sciences, (2): 42–44

Yao Ru, Cai Lina, Liu Jianqiang, et al. 2020. GF-1 satellite observations of suspended sediment injection of Yellow River Estuary, China. Remote Sensing, 12(19): 3126, doi: 10.3390/rs12193126

Ye Wei, Song Wei. 2020. Quantitative remote sensing monitoring of water quality in Bohai Bay based on Landsat multispectral data. E3S Web of Conferences, 206: 03007, doi: 10.1051/e3sconf/202020603007

Ye Yingying, Xu Meiying, Wu Changwen. 2011. Influences of some environmental factors on growth and survival of *mytilus coruscus gould* larvae. Journal of Zhejiang Ocean University (Natural Science) (in Chinese), 30(4): 292–296, doi: 10.3969/j.issn.1008-830X.2011.04.003

Yu Cungen, Chen Quanzhen, Chen Xiaoqing, et al. 2010. Species composition and quantitative distribution of fish in the Zhoushan fishing ground and its adjacent waters. Oceanologia et Limnologia Sinica (in Chinese), 41(3): 410–417

Yu Huijuan, Wang Jinhuan. 2015. From the strategic point of view, the construction of marine ranching should be emphasized and promoted. Rural Economy (in Chinese), (3): 50–53

Yu Cungen, Yan Xiaojun, Jiang Qiaoli, et al. 2022. Cause analysis of resources change and reconstruction strategy of *Larimichthys crocea* Daiqu group in the East China Sea. Journal of Fisheries of China (in Chinese), 46(4): 616–625, doi: 10.11964/jfc.20211013126

Yu Xiang, Yi Huapeng, Liu Xiangyang, et al. 2016. Remote-sensing estimation of dissolved inorganic nitrogen concentration in the Bohai Sea using band combinations derived from MODIS data. International Journal of Remote Sensing, 37(2): 327–340, doi: 10.1080/01431161.2015.1125555

Yuan Xinzhe, Lin Mingsen, Liu Jianqiang, et al. 2018. Application of GF-3 satellite in marine field. Satellite Application, (6): 17–21, doi: 10.3969/j.issn.1674-9030.2018.06.007

Zang Xi. 2018. Comparative study on fusion methods of GF-2 satellite image in land engineering application. China Western Developmen (in Chinese), 3(11): 7–12,17

Zhai Z K, Lu S L, Wang P, et al. 2021. Ocean Chlorophyll-*a* retrieval using GF1-WFV data—A case study of the central Bohai Sea. IOP Conference Series: Earth and Environmental Science, 626(1): 012021, doi: 10.1088/1755-1315/626/1/012021

Zhang Yihao. 2009. Study on shape comparison of mussel species in Zhejiang coast. Fisheries Economy Research (in Chinese), (2): 14–20, doi: 10.3969/j.issn.1674-9189.2009.02.004

Zhang Qing, Chen Peng. 2021. Application of gaofen No. 6 satellite in vegetation ecological remote sensing monitoring. Journal of Agriculture (in Chinese), 11(7): 56–59,111, doi: 10.11923/j.issn.2095-4050.cjas20191200315

Zhang Yi, Wang Chengyi, Ji Yuan, et al. 2020. Combining segmentation network and nonsubsampled contourlet transform for automatic marine raft aquaculture area extraction from sentinel-1 images. Remote Sensing, 12(24): 4182, doi: 10.3390/rs12244182

Zhang Tao, Yang Xiaomei, Hu Shanshan, et al. 2013. Extraction of coastline in aquaculture coast from multispectral remote Sensing images: object-based region growing integrating edge detection. Remote Sensing, 5(9): 4470–4487, doi: 10.3390/rs5094470